Cellular/Molecular

Analysis of Astroglial K$^+$ Channel Expression in the Developing Hippocampus Reveals a Predominant Role of the Kir4.1 Subunit

Gerald Seifert,[1] Kerstin Hüttmann,[1] Devin K. Binder,[2] Christian Hartmann,[1] Alexandra Wyczynski,[1] Clemens Neusch,[3] and Christian Steinhäuser[1]

[1]Institute of Cellular Neurosciences, University of Bonn, D-53105 Bonn, Germany, [2]Department of Neurological Surgery, University of California, Irvine, Irvine, California 92868-3298, and [3]Department of Neurology, University of Göttingen, D-37099 Göttingen, Germany

Astrocytes in different brain regions display variable functional properties. In the hippocampus, astrocytes predominantly express time- and voltage-independent currents, but the underlying ion channels are not well defined. This ignorance is partly attributable to abundant intercellular coupling of these cells through gap junctions, impeding quantitative analyses of intrinsic membrane properties. Moreover, distinct types of cells with astroglial properties coexist in a given brain area, a finding that confused previous analyses. In the present study, we investigated expression of inwardly rectifying (Kir) and two-pore-domain (K$_{2P}$) K$^+$ channels in astrocytes, which are thought to be instrumental in the regulation of K$^+$ homeostasis. Freshly isolated astrocytes were used to improve space-clamp conditions and allow for quantitative assessment of functional parameters. Patch-clamp recordings were combined with immunocytochemistry, Western blot analysis, and semiquantitative transcript analysis. Comparative measurements were performed in different CA1 subregions of astrocyte-targeted transgenic mice. While confirming weak Ba^{2+} sensitivity *in situ*, our data demonstrate that in freshly isolated astrocytes, the main proportion of membrane currents is sensitive to micromolar Ba^{2+} concentrations. Upregulation of Kir4.1 transcripts and protein during the first 10 postnatal days was accompanied by a fourfold increase in astrocyte inward current density. Hippocampal astrocytes from Kir4.1−/− mice lacked Ba^{2+}-sensitive currents. In addition, we report functional expression of K$_{2P}$ channels of the TREK subfamily (TREK1, TREK2), which mediate astroglial outward currents. Together, our findings demonstrate that Kir4.1 constitutes the pivotal K$^+$ channel subunit and that superposition of currents through Kir4.1 and TREK channels underlies the "passive" current pattern of hippocampal astrocytes.

Introduction

Astrocytes play a key role in the uptake of K$^+$ and neurotransmitters, thereby modulating synaptic and neurovascular signaling (Volterra and Meldolesi, 2005; Haydon and Carmignoto, 2006). Inwardly rectifying K$^+$ (Kir) channels aid redistribution of K$^+$ across glial membranes (Walz, 2000; Kofuji and Newman, 2004). In the CNS, Kir4.1 is specifically localized to astrocytes, oligodendrocytes, and retinal Müller cells (Takumi et al., 1995; Ishii et al., 1997; Kofuji et al., 2000; Poopalasundaram et al., 2000; Li et al., 2001; Neusch et al., 2001; Ishii et al., 2003; Olsen et al., 2006). Immunohistochemistry suggested preferred location of Kir4.1 on astroglial processes ensheathing synapses and blood vessels (Higashi et al., 2001). In astrocytes and Müller cells, Kir4.1 may assemble with Kir5.1, which confers pH sensitivity to the channels (Pessia et al., 1996; Tanemoto et al., 2000; Casamassima et al., 2003; Hibino et al., 2004).

Increasing evidence suggests that astrocytes comprise a heterogeneous cell population, with functional properties varying between brain regions. In the hippocampus, distinct types of cells with astroglial properties coexist. Hippocampal astrocytes (also termed GluT cells or passive cells) possess prominent time- and voltage-independent currents and, in contrast to cortical astrocytes (Lalo et al., 2006, 2008) or Bergmann glia (Clark and Barbour, 1997), display glutamate transporters but no ionotropic glutamate and ATP receptors (Steinhäuser et al., 1994; Zhou and Kimelberg, 2001; Matthias et al., 2003; Jabs et al., 2007). Astrocytes in the hippocampus are characterized by abundant coupling through gap junctions (Wallraff et al., 2004). Recent studies suggested that Kir4.1 is the major subunit mediating resting currents in Müller cells (Kofuji et al., 2000) and astrocytes in the spinal cord (Olsen et al., 2006) and brainstem (Neusch et al., 2005). However, contrary findings have been reported from the hippocampus. Here, the low sensitivity of astrocytic currents to Ba^{2+} and lacking inward rectification of the Ba^{2+}-sensitive component led to the idea that K$^+$ subunits other than Kir4.1 (e.g., two-pore-domain channels) (Päsler et al., 2007) substantially add to the cells' almost linear *I/V* relationships commonly observed in

whole-cell recordings *in situ* (Wallraff et al., 2004; Djukic et al., 2007). To further investigate this issue, we addressed the developmental regulation of Kir4.1 and expression of K_{2P} channels in murine hippocampal astrocytes by combining immunohistochemistry, Western blot analysis, single-cell reverse transcription (RT)-PCR, and patch-clamp analysis. We used transgenic mice possessing fluorescence labeling of astrocytes without and with Kir4.1 deletion. To improve recording conditions and allow for quantitative evaluation of membrane properties, freshly isolated astrocytes were used.

Materials and Methods

Tissue preparation for electrophysiology. Mice [transgenic human glial fibrillary acidic protein/enhanced green fluorescent protein (Tg(hGFAP/EGFP)) mice (Nolte et al., 2001); Kir4.1−/− mice (Kofuji et al., 2000) interbred with Tg(hGFAP/EGFP) mice; C57BL6J mice] of postnatal day 1 (P1) to P60 were anesthetized and killed by decapitation; their brains were dissected and washed, and the hemispheres were cut into 200-μm-thick slices in frontal orientation using a Vibratome (VT 1000S; Leica Microsystems). Slice preparation was performed at 6°C in Ca^{2+}-free HEPES-buffered external solution. Subsequently, slices were stored for at least 30 min in artificial CSF gassed by carbogen at room temperature (pH 7.4). Acutely isolated cells were obtained from slices after protease treatment as described previously (Matthias et al., 2003). Although suspended astrocytes retain the majority of their processes, it is likely that some distant tips are shorn off during isolation.

Recording setup and Ba^{2+} application. Recordings were obtained at P9–P12 (designated as P9) if not stated otherwise. Membrane currents were measured with the patch-clamp technique in the whole-cell configuration *in situ* as well as in freshly isolated cells. Current signals were amplified (EPC-7 or EPC-9 amplifier; HEKA), filtered at 3 and 10 kHz, and sampled at 10 and 100 kHz by an interface connected to a computer system, which also served as a stimulus generator. The resistance of the patch pipettes was 4 MΩ (borosilicate glass; Malsfeld). Capacitance and series resistance compensation (40–50%) were used to improve voltage-clamp control. Input resistance was determined by stepping the membrane from −70 to −60 mV. In slices, Ba^{2+} was added to the bath perfusion. K^+ channel blockers and modulators were applied to freshly isolated cells by transferring the cells with a tube electrode to different solutions (Seifert and Steinhäuser, 1995). The bath solution contained (in mM) 150 NaCl, 5 KCl, 2 $MgCl_2$, 2 $CaCl_2$, 10 HEPES, and 10 glucose, pH 7.4. The pipette solution was composed of (in mM) 130 KCl, 0.5 $CaCl_2$, 2 $MgCl_2$, 5 BAPTA, 10 HEPES, and 3 Na_2-ATP, pH 7.25. Recordings were obtained at room temperature. All reagents were purchased from Sigma unless otherwise stated. Arachidonic acid (AA) was suspended in DMSO (20 mM), aliquoted, and added to the bath solution immediately before use (final concentration of DMSO was 0.05%).

Immunohistochemistry. Mice were anesthetized with xylazine and ketamine and perfused intracardially with 4% paraformaldehyde (PFA)/PBS. Dissected brains were fixed overnight in 4% PFA/PBS at 4°C and cryoprotected in 30% sucrose. The brains were sliced into 50-μm-thick coronal sections. Endogenous peroxidase activity was quenched with 3% H_2O_2/PBS (1 h at room temperature), and slices were then incubated in 5% normal goat serum (NGS)/PBS for 1 h. The primary antibody (rabbit anti-Kir4.1; 1:200; Alomone Labs) was applied together with 0.3% Triton X-100 overnight at 4°C. After wash, horseradish peroxidase-conjugated goat anti-rabbit IgG was applied for 30 min (room temperature; 1:100 in 5% NGS/PBS). After wash, slices were incubated in Alexa Fluor 488-conjugated tyramide, diluted 1:100 in H_2O_2/amplification buffer according to the supplier's instruction (10 min at room temperature; Invitrogen). NeuroTrace 640/660 Nissl staining was performed (1:10 in PBS; Invitrogen) for 5 min (room temperature) according to the manufacturer's protocol. After wash in PBS, Vectashield mounting medium was applied, and slices were covered with coverslips.

For immunofluorescence double labeling, subsequent to fluorescence-conjugated tyramide, the second primary antibody was applied (mouse anti-GFAP; 1:100 in PBS; 3 h at room temperature). After wash, Alexa Fluor 594-conjugated goat anti-mouse antibody (1:200; In-

vitrogen) was applied (3 h at room temperature). After wash, the slices were mounted and covered. Multilabel immunofluorescence was visualized with confocal fluorescence microscopy (Fluoview FV1000; Olympus) at 10 and 60× magnifications.

Western blot. Whole hippocampi of mice at different ages (C57BL/6J: P3, P10, P21, P42, P60; Kir4.1−/−: P10) were homogenized in dissection buffer containing (in mM) 10 Tris-Cl, 250 sucrose, 2 Pefabloc (Roche). Homogenates were centrifuged at 11,000 × *g* for 10 min at 4°C to harvest membrane fractions. The pellet was resuspended in 2 vol of radioimmunoprecipitation assay buffer containing 50 mM Tris, 150 mM KCl, 1% Nonidet P-40, 1% sodium deoxycholate, 0.1% SDS, 1 mM EDTA, and 1 mM Pefabloc to dissolve membrane proteins. Undissolved components were removed by another centrifugation step at 1000 × *g* (2 min, 4°C). Protein concentration of the supernatant was determined by the copper/bicinchonic acid test using bovine serum albumin as a standard (Sigma). Equal amounts of protein were heated for 10 min at 45°C in SDS buffer containing 10 mM β-mercaptoethanol. Proteins were separated in 10% SDS-PAGE and blotted on polyvinylidene fluoride membranes. Blotted proteins were detected by means of immunolabeling using rabbit anti-Kir4.1 (1:400; Sigma) and goat anti-β-actin antibodies (1:250; Abcam), respectively (1 h at room temperature). Secondary antibodies were horseradish peroxidase-conjugated IgGs (1:5000; 20 min at room temperature; Dianova). Western blots were detected with a chemiluminescence assay (ECL reagent; GE Healthcare). After development of Roentgen films, protein bands were quantified with a CCD camera using AlphaEase software (Alpha Innotech).

Single-cell RT-PCR. Single-cell transcript analysis was performed as reported previously (Seifert et al., 1997; Matthias et al., 2003). Briefly, after recording (isolated cells), the cell at the tip of the pipette was transferred to a separate dish to be washed with fresh bath solution. The cell was aspirated into the recording pipette under microscopic control, and the cell content and ~3 μl of the pipette solution were expelled into a reaction tube containing 3 μl of DEPC-treated water. The reaction tube was frozen and stored at −80°C.

To prevent amplification of genomic DNA, RT-PCR was preceded by DNase treatment. Therefore, DNase mastermix containing first-strand buffer (Invitrogen), dithiothreitol (DTT; 10 mM), dNTPs (4× 250 μM; Applied Biosystems), RNasin (20 U; Promega), random hexamer primers (50 μM; Roche), and RNase-free DNaseI (10 U; Roche) were added to the frozen cell content in the reaction tube. The reaction mix (~10 μl) was covered with freshly aliquoted paraffin oil and incubated at 37°C (30 min), and DNaseI was heat inactivated at 95°C (5 min). Subsequently, reverse transcriptase (SuperscriptIII; 100 U; Invitrogen) and RNase inhibitor (20 U) were added, and the RT reaction was started (37°C, 1 h).

A multiplex two-round single-cell PCR was performed with primers for Kir2.x, Kir4.1, and Kir5.1 or for Kir4.1 together with K_{2P} channel primers (Table 1) (Schröder et al., 2002). The first PCR was performed after adding PCR buffer, $MgCl_2$ (2.5 mM), and primers (200 nM each) to the RT product (final volume, 50 μl). After denaturation, 5 U of *Taq* polymerase (Invitrogen) was added. Forty-five cycles were performed (denaturation at 94°C, 25 s; annealing at 49°C, 2 min for the first five cycles and 45 s for the remaining cycles; extension at 72°C, 25 s; final elongation at 72°C, 7 min). An aliquot (3 μl) of the PCR product was used as a template for the second PCR (35 cycles; annealing at 54°C, 2 min for the first 5 cycles and 45 s for the remaining cycles) using nested primers (Table 1). The conditions were the same as described for the first round, but dNTPs (4× 50 μM) and Platinum *Taq* polymerase (2.5 U; Invitrogen) were added. Products were identified with gel electrophoresis using a molecular weight marker (ΦX174 *Hinc*II digest; Eurogentec).

As a positive control, RT-PCR for single cells and for total RNA from mouse brain were run in parallel. To test for the efficiency of DNA degradation, PCR was performed without SuperscriptIII reverse transcriptase. Negative controls were performed using distilled water or bath solution for RT-PCR.

Cell harvesting and preparation of brain tissue for semiquantitative RT-PCR. Harvesting of cellular RNA from brain slices was performed as reported previously (Schröder et al., 2002). Briefly, the cell content was harvested by applying negative pressure to the pipette while retaining the gigaohm seal resistance between pipette tip and membrane. The flow of

Table 1. Primers for single-cell RT-PCR and sqRT-PCR

Gene	Sequence	Position	Product length	GenBank accession number
Kir4.1	se 5′-TATCAGAGCAGCCACTTCACCTTC	−32	570 bp	NM_020269
	as 5′-GGATCGTCTCGGCCCTCTTCTTAG	515		
Kir4.1 (nested)	se 5′-TTCACCTTCGAGCCAAGATGACG	−11	338 bp	
	as 5′-AGGCGTGTGGTTGGCAGGAG	302		
Kir5.1	se 5′-TGCAGATACTTACAGCCGACCAT	−136	407 bp	NM_010604
	as 5′-GGAGCCAAATATCAACCAGGAGA	248		
Kir5.1 (nested)	se 5′-CAGCCGACCATTGGACTGAG	−124	344 bp	
	as 5′-ACATATGGCGCCACTTGGTATC	199		
sq Kir4.1	se 5′-TTTATCAGAGCAGCCACTT	−34	72 bp	NM_020269
	as 5′-GTCGTCTGACTGTAATAG	21		
sq Kir4.1 (probe)	se FAM-5′-CCTTCGAGCCAAGATGACGTCGGTCGCTA-TAMRA	−13		
TWIK1	se 5′-GGCATCCCGTTCACCCTCCTCT	421	471 bp	NM_008430
	as 5′-GTCGTGCTCCATGATGTGAACCAG	868		
TWIK1 (nested)	se 5′-AGCCGCCGTGTTCTCTGT	597	272 bp	
	as 5′-GGTCTTCGTCCTTGTCTTTCTTC	846		
TREK1	se 5′-CAGCAAATAGTGGCAGCAATAAAC	310	373 bp	NM_010607
	as 5′-CCGCAGGGAGAGCCACAAAGAGGA	659		
TREK1 (nested)	se 5′-TCACTGGGACCTCGGAAGC	375	282 bp	
	as 5′-CAGCCAAACAGGATGAAGATGA	635		
TREK2	se 5′-ATCTTTGGGATCCCGCTTTTT	556	166 bp	NM_029911
	as 5′-AGCCAGCCAAGATGAAGAGAATC	699		
TREK2 (nested)	se 5′-GATCCCGCTTTTTGGTTTCT	564	126 bp	
	as 5′-ACCCGGATCTTGGTCTGG	672		
TRAAK	se 5′-CTCGGGGACCATCATCACTACCAT	291	256 bp	NM_008431
	as 5′-CAGGCAGCCGATCAGCAGGAAGA	524		
TRAAK (nested)	se 5′-TGCCGGGCGTCTCTTTTGTATCTT	345	159 bp	
	as 5′-ACCAGCCCCGGTGGCACAT	485		

se, Sense primer; as, antisense primer; sq, primers and probe for sqRT-PCR analysis. Position 1 is the first nucleotide of the initiation codon. The Kir4.1 TaqMan probe was labeled with FAM (6-carboxyfluorescein; 5′ end) and TAMRA (6-carboxytetramethylrhodamine; 3′ end). All Kir and K_{2P} sense and antisense primers are located on different exons, respectively.

the cytoplasm into the pipette was controlled via a CCD camera (C-5405; Hamamatsu Photonics). The cell on top of the pipette was lifted above the slice and completely harvested in the flow of the bath solution under visual control. Only single cells without any adherent tissue debris were selected for analysis. Four to five cells were pooled in the same tube (see above; final volume, ~10 μl) for semiquantitative RT-PCR (sqRT-PCR) analysis. Oligo(dT)$_{25}$-linked Dynabeads (Dynal) were used to isolate mRNA from cytoplasmic content. Lysis buffer (20 μl) and Dynabeads suspended in lysis buffer (10 μl) were added to the reaction tube. After wash (50 μl), the beads with adherent mRNA were suspended in water (20 μl), frozen, and stored at −80°C until sqRT-PCR.

Tissue samples were isolated from 200-μm-thick coronal brain slices. By using a stereo microscope, the CA1 region was isolated with a small scalpel, by removing strata pyramidale and oriens. For regional comparison, in some cases the radiatum of the CA1 region was separated from the lacunosum-moleculare; otherwise, combined radiatum plus lacunosum-moleculare samples underwent sqRT-PCR analysis. By P3, the entire CA1 region was used because separation of pyramidal layer and oriens was not possible. At each developmental stage, at least three mice from different litters were used, and at least three sections were investigated in each mouse. Total RNA was isolated from tissue samples with Trizol (Invitrogen) and dissolved in 10 μl of DEPC-treated water. Genomic DNA was removed by DNase treatment in a mixture containing PCR buffer, 2.5 mM MgCl$_2$, 10 mM DTT (all from Invitrogen), 20 U of DNaseI (Roche), and 40 U of RNase inhibitor (final volume, 20 μl; incubation at 37°C for 30 min; Promega). Subsequently, mRNA was isolated using oligo(dT)$_{25}$-linked Dynabeads (Dynal), and beads with the adherent mRNA were suspended in DEPC-treated water (20 μl), frozen, and stored at −80°C.

sqRT-PCR. RT-PCR was performed as a single enzyme procedure using recombinant *Thermus thermophilus* (rTth) DNA polymerase (TaqMan EZ RT-PCR kit; Applied Biosystems). The reaction volume was 12.5 μl. The reaction mixture contained TaqMan EZ buffer, 3× 300 μM dNTPs (dATP, dCTP, dGTP), 600 μM dUTP, 3 mM Mn(OAc)$_2$, 1.25 U of rTth DNA polymerase, and 0.125 U of uracil-*N*-glycosylase. For Kir4.1 sqRT-PCR analysis, 100 nM fluorogenic TaqMan probe and 300 nM of

each primer was added (Table 1). For β-actin detection and quantification, a TaqMan probe/primer mix was used (Applied Biosystems). For sqRT-PCR analysis of cell pools, aliquots of 4 μl of mRNA were added to each tube. Investigating developmental changes of Kir4.1 expression with mRNA from tissue samples, 0.5 μl of mRNA was added. RT-PCRs for Kir4.1 and β-actin were run in parallel tubes for each sample, respectively. Negative controls (water) and positive controls (mRNA from mouse brain) were also performed in each run. Samples were incubated at 50°C (2 min), and first-strand synthesis was performed at 60°C (20 min). After denaturation (95°C, 5 min), 50 or 60 cycles were performed (denaturation at 94°C, 15 s; primer annealing and extension at 59°C, 60 s). Fluorescence intensity was read out during each annealing/extension step.

Data analysis. Total membrane conductance was determined according to the following equation:

$$g_{mem} = I_{-130mV}/(-130mV - V_R) \text{ or } I_{+20mV}/(+20mV - V_R), \quad (1)$$

where $I_{-130\,mV}$ ($I_{+20\,mV}$) is the membrane current at −130 and +20 mV, respectively. V_R is the resting membrane potential.

The rectification index (RI) of Ba^{2+}- and quinine-sensitive currents was determined by comparing the chord conductance of blocker-sensitive currents at −40 and −130 mV (5 mM [K$_o$]$^+$; Eq. 2a) or +20 and −70 mV (50 mM [K$^+$]$_o$; Eq. 2b) according to the following:

$$RI = [I_{-40mV}/(-40mV - E_{rev})]/[I_{-130mV}/(-130mV - E_{rev})], \quad (2a)$$

$$RI = [I_{+20mV}/(+20mV - E_{rev})]/[I_{-70mV}/(-70mV - E_{rev})], \quad (2b)$$

where I is the amplitude of Ba^{2+}-sensitive currents at +20, −40, −70, and −130 mV, respectively, and E_{rev} its extrapolated reversal potential.

The K_D for Ba^{2+} was determined according to the following equation:

$$g_{-130mV,Ba} = g_{-130mV,control}[1/1 + ([Ba^{2+}]/K_D)^{nH}], \quad (3)$$

where $g_{-130\,mV,Ba}$ is the total membrane conductance at −130 mV at the respective Ba^{2+} concentration [Ba^{2+}], $g_{-130\,mV,control}$ is the membrane conductance before Ba^{2+} application, K_D is the concentration at half-

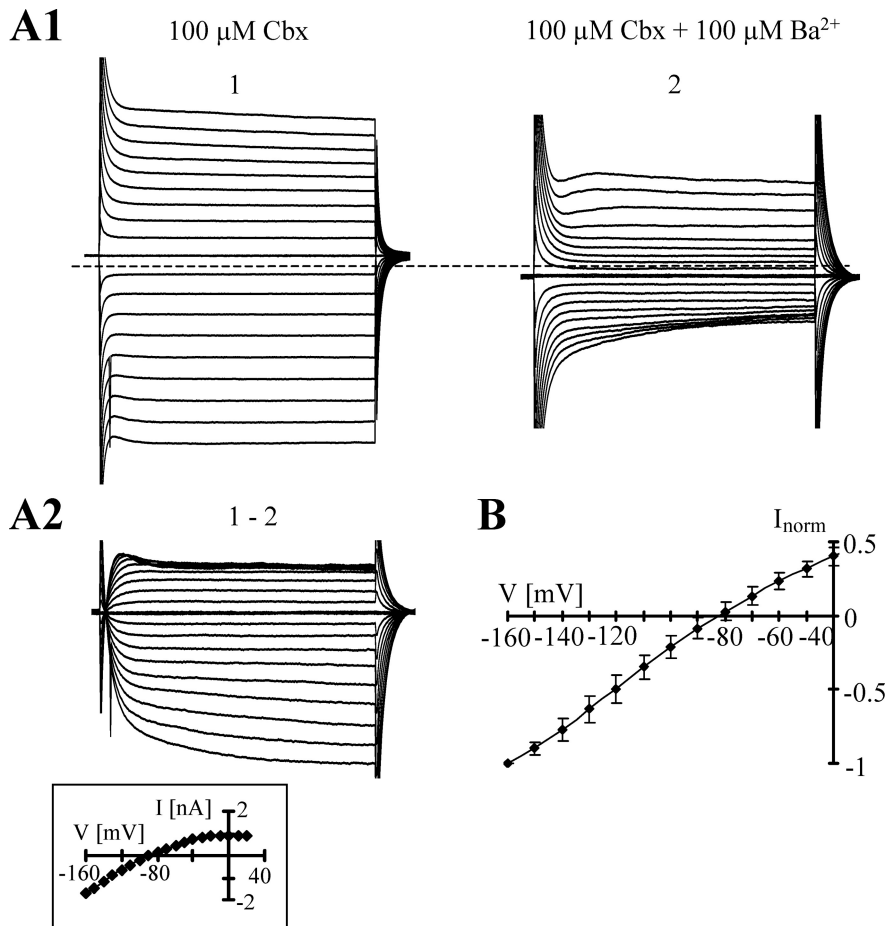## A1

100 μM Cbx

100 μM Cbx + 100 μM Ba²⁺

A2

1 - 2

B

Figure 1. Block of membrane currents of astrocytes *in situ* by Ba²⁺ in the presence of Cbx (100 μM). **A1**, Membrane currents were elicited in the whole-cell mode by depolarization and hyperpolarization between −160 and +20 mV (1; 10 mV increments; holding potential, −70 mV; dashed line, zero current). After adding 100 μM Ba²⁺ to the bath, currents were reduced (2). **A2**, Ba²⁺-sensitive currents were determined by subtracting respective current families (1–2). Ba²⁺-sensitive currents (inset) reversed at −88.5 mV. **B**, The averaged *I/V* relationship of Ba²⁺ (100 μM)-sensitive currents obtained in the presence of Cbx of six astrocytes (mean ± SD). In each cell, data were normalized to maximum inward currents.

Table 2. Resting membrane potential and input resistance of astrocytes *in situ* under control conditions and after adding Ba²⁺

Age	Resting potential (mV)	Input resistance (MΩ)
P9, control	−71.9 ± 3.4 (*n* = 10)	38.7 ± 17.0 (*n* = 10)
P9, 100 μM Cbx	−71.9 ± 1.6 (*n* = 6)	44.2 ± 17.5 (*n* = 6)
P9, 100 μM Cbx, 100 μM BaCl₂	−61.0 ± 4.1[a] (*n* = 6)	93.3 ± 49.8[a] (*n* = 6)
P9, Kir4.1−/−	−39.1 ± 9.8[b] (*n* = 9)	143.0 ± 82.4[b] (*n* = 9)
P9, Kir4.1−/−, 100 μM BaCl₂	−38.3 ± 10.1 (*n* = 9)	140.5 ± 54.3 (*n* = 9)

Data were obtained from hGFAF/EGFP mice and from Kir4.1−/− mice crossed with hGFAP/EGFP mice. Cell numbers are given in parentheses.

[a]In the presence of Cbx (100 μM; 30 min preincubation), Ba²⁺ significantly affected resting potential and input resistance.

[b]In addition, resting potential and input resistance of astrocytes in control versus Kir4.1−/− mice differed significantly.

maximal conductance inhibition at −130 mV, and n_H is the Hill coefficient.

The Kir4.1/β-actin gene expression ratio was determined by comparing C_T values of the target gene with those of the reference gene, β-actin. The relative quantification of different genes was determined according to the following equation:

$$Y = X^*E^{CT}$$ or, in the logarithmic form,

$$\log Y = \log X + C_T{}^*\log E, \quad (4)$$

where *Y* is the amount of the PCR product, *X* is the input copy number, *E* is the efficiency of amplification, and C_T is the cycle number at threshold. According to Equation 4, the fluorescence intensity, R_n, which is proportional to *Y*, was determined at each cycle. By quantification of Kir4.1, gene expression against that of β-actin C_T was determined for each gene at the same R_n, and the difference in input copy number was estimated according to Equation 5:

$$X_{Kir41}/X_{\beta\text{-actin}} = E_{\beta\text{-actin}}{}^{CT\beta\text{-actin}}/E_{Kir4.1}{}^{CTKir4.1}.$$

$$(5)$$

The amplification efficiency was 1.93 for Kir4.1 and 1.97 for β-actin (supplemental Fig. 1, available at www.jneurosci.org as supplemental material).

Results

Ba²⁺-sensitive inward currents in hippocampal astrocytes *in situ*

GluT cells in the hippocampus of Tg(hG-FAP/EGFP) mice were identified according to their morphological and functional properties as reported previously (Matthias et al., 2003; Wallraff et al., 2004; Jabs et al., 2005). These cells resemble the "passive cells" first described in the hippocampus of wild-type mice (Steinhäuser et al., 1992, 1994) and can be considered *bona fide* gray matter astrocytes.

Previous work has revealed that currents through gap junctions add to the passive membrane conductance of astrocytes (Blomstrand et al., 2004). Actually, a 30% decline of astrocytic membrane conductance was observed when the recordings were obtained at low pH or in bath solutions containing low bicarbonate concentrations (i.e., conditions known to inhibit currents through gap junctions) (Wallraff et al., 2006). After preincubation (30 min) of slices in a solution supplemented with 100 μM carbenoxolone (Cbx), a blocker of gap junctions and connexin hemichannels, bath application of Ba²⁺ (100 μM) reduced the membrane conductance by 54.0 ± 13.6% (−130 mV; *n* = 6), increased input resistance, and shifted V_R from −71.9 ± 1.6 to −61.0 ± 4.1 mV compared with the Cbx control (Fig. 1; Table 2). The *I/V* relationship of Ba²⁺-sensitive currents displayed weak inward rectification (RI, 0.66 ± 0.09) (Fig. 1*A2*,*B*), with a reversal potential E_{rev} = −84.1 ± 5.4 mV, which was close to E_K (−82.3 mV).

Hence, a significant proportion of the voltage- and time-independent currents of astrocytes apparently were insensitive to submillimolar Ba²⁺ concentration. However, membrane current analysis in astrocytes *in situ* is not only compromised by gap junction coupling but also by the limited special and temporal voltage-clamp control caused by the extensive branching of these cells. It has also to be considered that addition of Ba²⁺ to slices increases the extracellular K⁺ concentration (Heinemann et al., 2000), which disturbs quantification of astrocyte K⁺ currents *in situ*. Therefore, to improve recording conditions and address the question to what extent currents through Kir channels contribute to the intrinsic
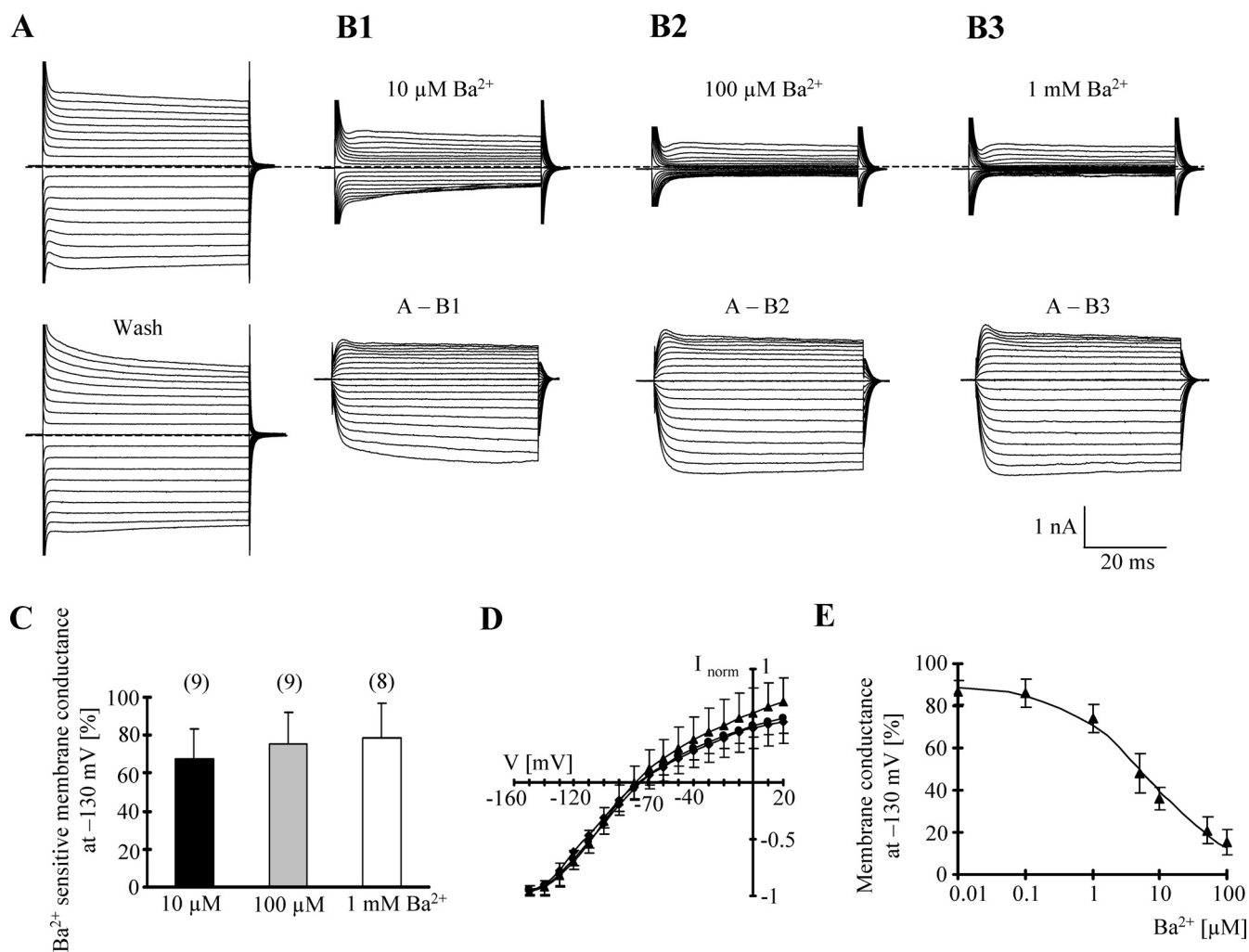
Figure 2. Ba^{2+} sensitivity of freshly isolated astrocytes. **A**, Membrane currents were elicited as described in Figure 1. The bottom panel shows the responses after washout of Ba^{2+}. **B1–B3**, Current responses after increasing concentrations of Ba^{2+}. Ba^{2+}-sensitive currents (bottom) were determined by subtracting current traces obtained in Ba^{2+} from those before Ba^{2+} application at respective voltages. **C**, Membrane conductance in control and Ba^{2+}-containing solution was determined at −130 mV according to Equation 1, and Ba^{2+}-sensitive fractions were determined at different concentrations of the blocker. **D**, Mean *I/V* relationships of blocker-sensitive currents in 0.01 mM Ba^{2+} (diamonds; $n = 9$), 0.1 mM Ba^{2+} (circles; $n = 9$), and 1 mM Ba^{2+} (triangles; $n = 8$). In each cell, data were normalized to maximum inward current. **E**, Mean dose–inhibition curve of membrane conductance ($n = 7$). Half-maximal inhibition occurred at a Ba^{2+} concentration of 7.1 ± 3.2 μM, with a Hill coefficient of $n_H = 0.7 ± 0.1$. Data in **C–E** are given as mean ± SD; cell numbers are in parentheses.

Table 3. Cell capacitance, resting membrane potential, and input resistance of isolated astrocytes under control conditions and after addition of BaCl$_2$

Age	Cell capacitance (pF)	RMP (mV)	Input resistance (MΩ)	RMP (mV) 10 μM BaCl$_2$	RMP (mV) 100 μM BaCl$_2$	RMP (mV) 1 mM BaCl$_2$
P3	14.2 ± 6.2 ($n = 9$)	−59.6 ± 9.2 ($n = 9$)	288 ± 109[b] ($n = 9$)	−46.7 ± 15.0 ($n = 7$)	−39.6 ± 12.2[a] ($n = 9$)	−23.0 ± 6.1[a] ($n = 5$)
P10	10.3 ± 4.3 ($n = 10$)	−65.0 ± 6.4 ($n = 10$)	98 ± 69 ($n = 10$)	−54.7 ± 10.0[a] ($n = 9$)	−42.3 ± 8.7[a] ($n = 9$)	−25.1 ± 7.9[a] ($n = 8$)
P10 (at pH 6.5)	15.0 ± 6.9 ($n = 12$)	−60.8 ± 4.9 ($n = 12$)	63 ± 51 ($n = 12$)		−41.0 ± 9.8[a] ($n = 12$)	
P10 Kir4.1−/−	31.0 ± 17.0[c] ($n = 10$)	−23.6 ± 6.8[c] ($n = 10$)	417 ± 359[c] ($n = 10$)	−26.8 ± 7.5[d] ($n = 8$)	−24.7 ± 9.4[d] ($n = 10$)	−20.9 ± 6.1 ($n = 9$)

RMP, Resting membrane potential. Data were obtained from hGFAF/EGFP mice and Kir4.1 knock-out mice crossed with hGFAP/EGFP mice. Cell numbers are given in parentheses.

[a]Significant changes after BaCl$_2$ application at P10 and P3, respectively.

[b]Significant higher input resistance at P3 compared with P10 mice.

[c]Cell capacitance, RMP, and input resistance were significantly different between hGFAP/EGFP mice and Kir4.1−/− mice at P10.

[d]The RMP of astrocytes from Kir4.1−/− mice in 10 and 100 μM BaCl$_2$ solution was significantly depolarized to those of wild-type GFAP/EGFP mice in Ba^{2+} solution, compared the same column, respectively.

membrane conductance of astrocytes, further investigation was performed with freshly isolated cells.

Properties of inwardly rectifying currents in freshly isolated hippocampal astrocytes

After acute isolation, brightly fluorescent astrocytes with extended branching were selected for recording. In addition, astro-cytic identity was confirmed by evoking glutamate transporter currents (data not shown) (Matthias et al., 2003). Ba^{2+} pro-foundly reduced both inward and outward currents in these cells (Fig. 2*A*,*B*) and caused a positive shift of V_R (Table 3). At −130 mV, membrane conductance declined by 67.3 ± 12.9% ($n = 9$), 75.5 ± 12.8% ($n = 9$), and 78.2 ± 12.4% ($n = 8$) at 10 μM, 100 μM, and 1 mM Ba^{2+}, respectively (Fig. 2*C*). Currents blocked by

100 μM Ba^{2+} reversed at -75.4 ± 6.5 mV ($n = 9$) (i.e., close to E$_K$) (Fig. 2D). The corresponding I/V curves normalized to maximal inward currents indicated intermediate rectification (RI, 0.58 ± 0.13). To determine the potency of Ba^{2+} at blocking membrane currents in astrocytes, the membrane conductance was determined at -130 mV in solutions with increasing Ba^{2+} concentrations (10 nM to 100 μM). Half-maximal inhibition of the conductance occurred at a Ba^{2+} concentration of 7.1 ± 3.2 μM ($n = 7$) (Fig. 2E). The Hill coefficient amounted to $n_H = 0.7 \pm 0.1$.

pH sensitivity of inward currents in isolated astrocytes
Next, we tested the pH sensitivity of inward currents in astrocytes. For comparison, the Ba^{2+} sensitivity was tested in the same cell. Previous work has demonstrated coexpression of Kir4.1 together with Kir5.1 in astrocytes and Müller cells (Ishii et al., 2003; Hibino et al., 2004), and the subunit Kir5.1 was shown to confer high pH sensitivity to Kir4.1 channels. Activity of heteromeric Kir4.1/Kir5.1 channels is significantly reduced by acidic pH (Tanemoto et al., 2000; Xu et al., 2000). In contrast, inward currents in retinal Müller glial cells are highly pH sensitive because of the expression of acid-sensitive two-pore-domain K$^+$ channels (Skatchkov et al., 2006).

Astrocytes were exposed to acidic bath solution (pH 6.5), and then 100 μM Ba^{2+} was added to the same solution (supplemental Fig. 2A,B, available at www.jneurosci.org as supplemental material). Under these conditions, the membrane conductance declined by $7.5 \pm 6.5\%$ ($n = 12$; pH 6.5; -130 mV) and $70.3 \pm 12.2\%$ ($n = 12$; pH 6.5 with 100 μM Ba^{2+} added) compared with control currents at pH 7.4 (supplemental Fig. 2C, available at www.jneurosci.org as supplemental material). Treatment of cells with acidic pH did not shift V_R ($\Delta V_R = 2.1 \pm 2.7$ mV) (Table 3), whereas channel block by 100 μM Ba^{2+} led to a depolarization by 22.0 ± 8.8 mV (Table 3). Comparing current densities at -130 mV, in a given cell the pH-sensitive component amounted only to 3% of the Ba^{2+}-sensitive component (supplemental Fig. 2D, available at www.jneurosci.org as supplemental material). Ba^{2+}-sensitive currents displayed an E_{rev} of -75 ± 5.6 mV (RI, 0.69 ± 0.16; $n = 12$). The small pH-sensitive component also reversed close to E_K (reversal at -81 ± 10 mV).

Kir transcript analysis in astrocytes of the hippocampus
Previous data suggested abundant expression of Kir4.1 in glial cells of the CNS (Takumi et al., 1995; Poopalasundaram et al., 2000; Hibino et al., 2004; Olsen et al., 2006). In the hippocampus, complex glial cells weakly express Kir4.1 (Schröder et al., 2002), but the identity of inward currents in astrocytes of that brain region has not been resolved yet. To investigate which Kir subunits are expressed by hippocampal astrocytes, patch-clamp analysis was combined with postrecording single-cell RT-PCR. Kir4.1 transcripts were found in all cells tested ($n = 39$). All astrocytes coexpressed Kir4.1 together with AQP4 ($n = 11$; data not shown), an astroglial water channel (Nagelhus et al., 2004; Dibaj et al., 2007). Transcripts encoding Kir5.1 were rarely found. Six of 33 cells (18%) expressed Kir5.1, either with Kir4.1 ($n = 4$ of 16) or with AQP4 ($n = 2$ of 17) (Fig. 3). Coexpression of subunits of the Kir2.0 family together with Kir4.1 was tested in 26 astrocytes. Kir2.3 transcripts were found in half the Kir4.1-positive cells, Kir2.1 was found in six cells (23%), and Kir2.2 was found in eight cells (31%). Nine Kir4.1-positive cells (35%) were devoid of Kir2.0 transcripts. In summary, among the constitutively active Kir channels (Kir2.1–Kir2.3, Kir4.1, Kir5.1), only Kir4.1 showed invariable expression in hip-

pocampal astrocytes, whereas transcripts for the other subunits were only occasionally present (Fig. 3).

Upregulation of Kir4.1 protein expression in hippocampal astrocytes during postnatal development
To corroborate expression of Kir4.1 protein in hippocampal astrocytes, immunohistochemistry was applied. Specificity of the commercially available Kir4.1 antibody was tested by staining hippocampal slices from Kir4.1$-/-$ mice, which lacked Kir4.1 immunoreactivity (Fig. 4A; supplemental Fig. 3A, available at www.jneurosci.org as supplemental material). In wild-type mice aged P3–P42, Kir4.1/GFAP-positive cells were found in strata radiatum, lacunosum-moleculare, and oriens of the CA1 region as well as in the stratum moleculare and the hilus of the dentate gyrus (Fig. 4B–D; supplemental Fig. 3B–D, available at www.jneurosci.org as supplemental material). In the pyramidal layer of the CA1 region and the granular layer of the dentate gyrus, only Kir4.1-positive fibers were discerned, whereas the somata (labeled by Nissl staining) were Kir4.1 negative (supplemental Fig. 3B–D, available at www.jneurosci.org as supplemental material). Perinatally (P3), the number of GFAP-positive cells in the hippocampus was very low (Fig. 4B). Together, these data indicated astroglial localization of Kir4.1 and a developmental upregulation of this protein in the postnatal hippocampus.

Quantification of developmental Kir4.1 regulation by real-time RT-PCR and Western blot
To confirm the immunofluorescence data and to quantify the developmental increase in Kir4.1, real-time RT-PCR was performed with mRNA isolated from whole hippocampal slices. The "housekeeping" gene β-actin served as an internal standard. Figure 5A compares amplification curves of Kir4.1 and β-actin mRNA from the CA1 region at P3 and P21. At P3, more PCR cycles were necessary to reach a given threshold level, indicating a lower initial Kir4.1 copy number compared with P21. To get a quantitative measure, the threshold cycle differences, ΔC_T, between Kir4.1 and β-actin were determined in individual samples, and the gene ratios, Kir4.1/β-actin, were calculated according to Equation 5. At P3, the Kir4.1/β-actin mRNA ratio was 1:134 (0.00748 ± 0.0022; $n = 12$), whereas at P21, the ratio amounted to 1:24 (0.0391 ± 0.0189; $n = 10$), indicating a sixfold increase in Kir4.1 transcript content during that period (Fig. 5B). The differences in mRNA expression ratio between P1 and P10–P60 and between P3 and P10–P60 were significant (one-way ANOVA, Tukey's *post hoc* test, $p < 0.01$). A plateau of Kir4.1 mRNA levels in the CA1 region of the hippocampus was already reached at P10 (Fig. 5B).

Next we compared the developmental regulation of Kir4.1 transcripts within different CA1 subareas. Between P10 and P60, individual strata radiatum and lacunosum-moleculare were isolated and analyzed separately. Between P21 and P60, the Kir4.1/β-actin ratio of the stratum lacunosum-moleculare exceeded that of the radiatum threefold to fourfold, whereas no differences were found at P10 (Student's t test, $p < 0.05$) (supplemental Fig. 4A,B,D, available at www.jneurosci.org as supplemental material).

To analyze Kir4.1 expression in single cells, the cytoplasm of four or five astrocytes was harvested and pooled, mRNA was isolated, and real-time sqRT-PCR was performed as described above. In P3 astrocytes, the Kir4.1/β-actin ratio amounted to 1:14 (0.0719 ± 0.0652; $n = 6$ cell pools) and increased 2.5-fold at later ages (P12–P43, 0.1850 ± 0.0822, $n = 8$; one-way ANOVA,

Tukey's *post hoc* test, $p < 0.05$) (supplemental Fig. 4*C,D*, available at www.jneurosci.org as supplemental material).

Postnatal changes in Kir4.1 protein content displayed a time course similar to the developmental switch in transcript expression (Fig. 5*C,D*). Membrane fractions (i.e., receptor tetramers; $n = 6$) (Fig. 5*C1*) were analyzed by Western blot under denaturing conditions. Blots were analyzed separately (seven mice at each age), and gel loading was calibrated to β-actin. Before quantitative evaluation, specificity of the putative Kir4.1 monomer and tetramer bands was tested using Kir4.1−/− mice. In these mice, no signals were observed at 43 and 160 kDa, respectively (Fig. 5*C2*). After calibration of gray levels of Kir4.1 with respect to the β-actin signal of the same sample, Kir4.1 optical densities obtained at different ages were normalized to the P42 value. A significant increase in Kir4.1 protein was observed between P3 and P60 (Fig. 5*D*) (one-way ANOVA, Tukey's *post hoc* test, $p < 0.01$). Compared with P3, Kir4.1 tetramer protein increased 13- and 40-fold at P12 and P42, respectively (Fig. 5*C1,D*).

Inwardly rectifying currents in astrocytes from perinatal mouse hippocampus

Both antibody staining and transcript analysis indicated weak expression of Kir4.1 perinatally and profound upregulation between P3 and P12. For functional characterization of astrocytes between P1 and P3 (designated as P1), freshly isolated EGFP-positive cells with typical extended processes lacking ionotropic glutamate receptor responses were selected. Notably, the current patterns of these immature cells displayed strong outward rectification, as opposed to the more linear or inwardly rectifying current phenotype observed beyond P9 (compare Figs. 2, 3, 6). Although the resting membrane potential of perinatal astrocytes was similar to P9 astrocytes, a significantly higher input resistance was noted at P1 (Table 3), which was attributable to much smaller K^+ inward current (Fig. 6*A,E*). In Ba^{2+}-containing solutions, the inward conductance at −130 mV was reduced by the same amount as in P9 astrocytes (10 μM Ba^{2+}, by 68.8 ± 7.2%, $n = 7$; 100 μM Ba^{2+}, by 75.5 ± 8.7%, $n = 9$; 1 mM Ba^{2+}, by 77.0 ± 8.3%, $n = 5$) (Fig. 6*C*; see also Fig. 2*C*). Similarly, the RI value (0.65 ± 0.19; $n = 9$) and V_{rev} (−68.6 ± 6.5 mV) of currents sensitive to 100 μM Ba^{2+} did not differ from P9 cells (compare Fig. 2*D*). However, the amplitude of Ba^{2+}-sensitive inward currents was smaller in perinatal astrocytes. This is illustrated in Figure 6*E*, which compares the Ba^{2+} (100 μM)-sensitive current densities of P1 and P9
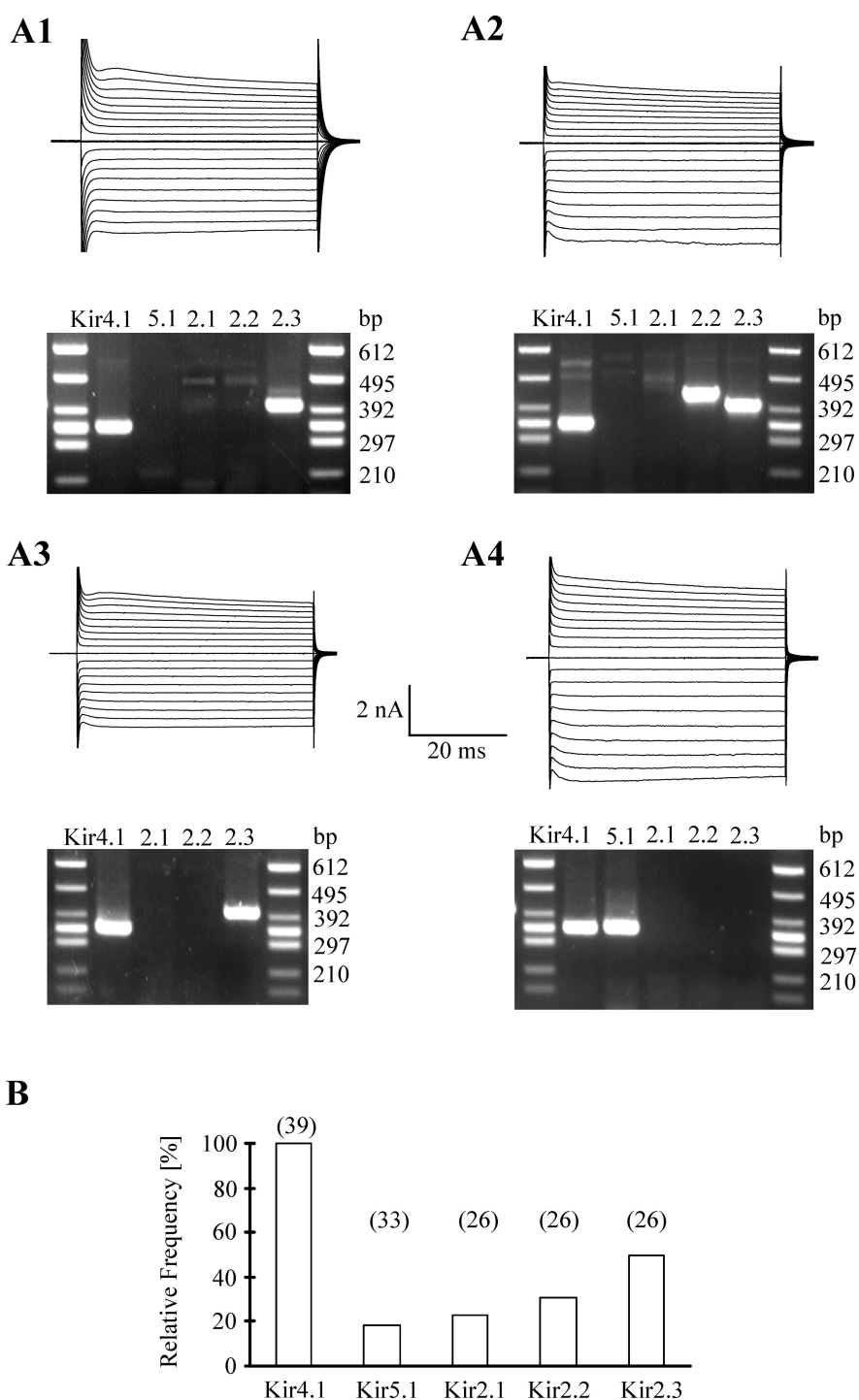

Figure 3. Analysis of Kir expression in single astrocytes. *A1–A4*, Cells were depolarized and hyperpolarized by 90 mV (10 mV increments) from a holding potential of −60 mV (*A2*) or −70 mV (*A1, A3, A4*). After recording, the cell content was harvested, and RT-PCR was performed. Kir4.1 was coexpressed with other Kir subunits as shown in the agarose gels below the respective current pattern. The expected product lengths were 338 bp for Kir4.1, 344 bp for Kir5.1, 408 bp for Kir2.1, 437 bp for Kir2.2, and 401 bp for Kir2.3. *B*, Summary of Kir detection in single astrocytes. The number of cells tested is given in parentheses.

astrocytes. At −130 mV, the current density of perinatal astrocytes reached only 26.7% of the cells at P9.

Astrocytes from Kir4.1−/− mice lack Ba^{2+}-sensitive inward currents

To confirm that Kir4.1 mediates the bulk of Ba^{2+}-sensitive inward current in hippocampal astrocytes, Kir4.1−/− mice were
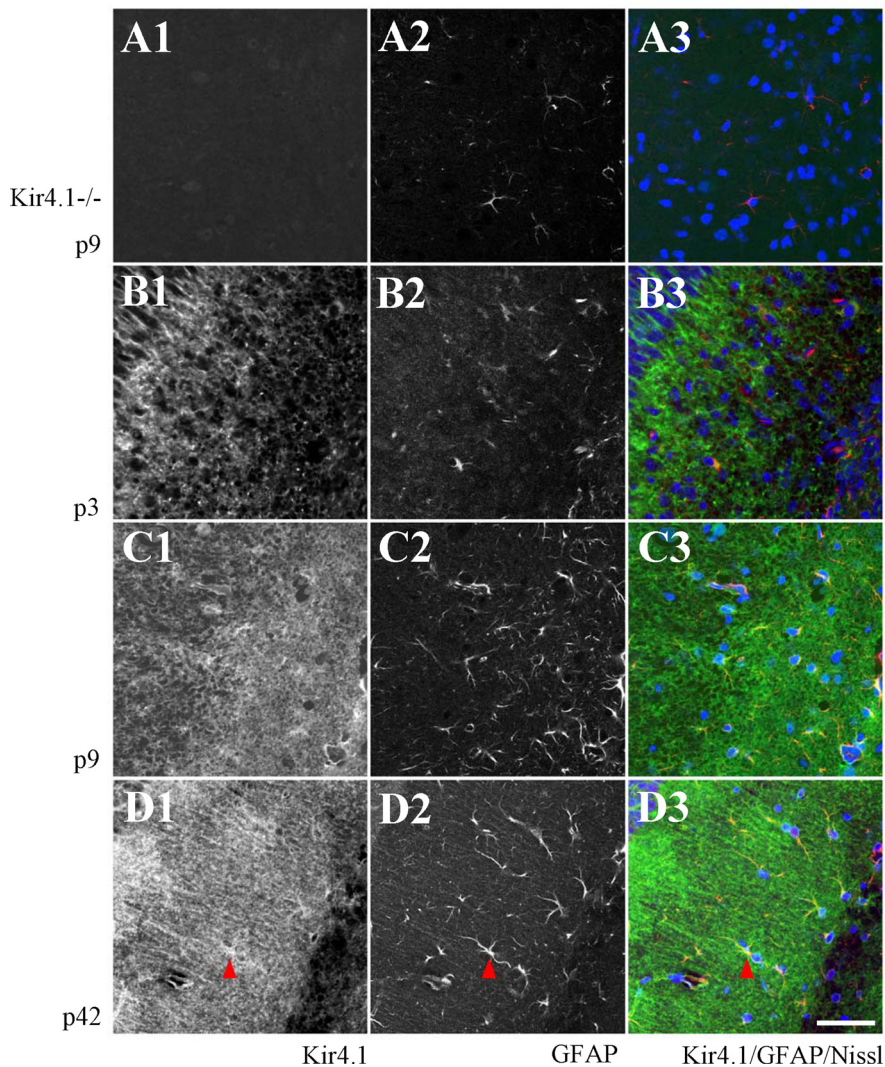
Figure 4. Confocal analysis of colabeling of Kir4.1 and GFAP in strata radiatum and lacunosum-moleculare of the developing CA1 region. *A1*, Kir4.1 immunoreactivity was absent in Kir4.1−/− mice. *A2*, GFAP staining in the same section. *A3*, The merge along with Nissl staining (blue; GFAP is in red). *B–D*, Kir4.1 immunoreactivity (*B1*, *C1*, *D1*), GFAP staining (*B2*, *C2*, *D2*), and the merge along with Nissl counterstaining (*B3*, *C3*, *D3*) at P3, P9, and P42 as indicated (Kir4.1, green). Red arrowheads (*D*) indicate colocalization of Kir4.1 and GFAP. Scale bar, 50 μm. In the top left, part of the pyramidal layer is visible.

current amplitudes (Fig. 8). The resting potential of Kir4.1−/− astrocytes was more depolarized compared with wild-type astrocytes after Cbx incubation and Ba^{2+} block, indicating that the Kir blocker probably failed to completely inhibit K$^+$ resting currents *in situ*.

Expression of two-pore-domain K$^+$ (K$_{2P}$) channels by hippocampal astrocytes?

So far, our experiments demonstrate that the membrane conductance of hippocampal astrocytes is mainly, although not exclusively, mediated by Kir4.1 channels. It has been suggested that astrocytes also express K$_{2P}$ channels. To test for functional expression of K$_{2P}$ channels, the inhibitors quinine and bupivacaine (200 μM each) (Lesage and Lazdunski, 2000) were applied to isolated astrocytes. Quinine led to a profound reduction of inward and outward currents (supplemental Fig. 5A, available at www.jneurosci.org as supplemental material) and significantly depolarized the membrane (shift of V_R from −66.7 ± 2.9 to −29.2 ± 21.5 mV; $n = 7$). The quinine-sensitive current fraction amounted to 63 ± 13% (at −130 mV), which was similar to the Ba^{2+}-sensitive component of isolated astrocytes determined at the same age (compare Fig. 2C). Quinine-sensitive currents reversed at −71.2 ± 2.9 mV and displayed slight outward rectification (RI, 1.18 ± 0.23; $n = 7$). In contrast, the local anesthetic bupivacaine did not affect V_R in the same cells (−59.7 ± 11.0 mV; $n = 7$) while reducing the membrane conductance by 35.8 ± 18% (−130 mV). Bupivacaine-sensitive currents reversed at −72.6 ± 4.6 mV and showed outward rectification (RI, 1.44 ± 0.72; $n = 7$) (supplemental Fig. 5B, available at www.jneurosci.

used. To facilitate identification of astrocytes in Kir4.1−/− mice, the latter were crossed with Tg(hGFAP/EGFP) mice, and the offspring were characterized by genotyping. Cells were freshly isolated from the hippocampus. Kir4.1−/−;EGFP-positive astrocyte cells with prominent processes were selected and analyzed in the whole-cell mode. At P9, these cells displayed outwardly rectifying current patterns (Fig. 7A) and high-input resistances and strongly depolarized resting membrane potentials, resembling age-matched control cells recorded in 1 mM Ba^{2+} solution (Table 3). Application of Ba^{2+} to astrocytes from Kir4.1−/−;Tg(hGFAP/EGFP) mice failed to block inward currents and did not change V_R (Table 3; Fig. 7B,C).

To confirm that Ba^{2+}-sensitive inward currents are also abolished in Kir4.1−/− astrocytes *in situ*, EGFP-positive cells were recorded in acute hippocampal brain slices of Kir4.1−/−;Tg(hGFAP/EGFP) mice. As expected, these slice recordings revealed depolarized V_R values and higher input resistances compared with control cells from Tg(hGFAP/EGFP) mice (Table 2). Bath application of Ba^{2+} (100 μM) to Kir4.1−/− astrocytes *in situ* did not affect resting potential, input resistance (Table 2), or K$^+$

org as supplemental material). Since both blockers, quinine and bupivacaine, significantly reduced inward currents, presumably through block of Kir channels, Ba^{2+} (100 μM) was applied before the K$_{2P}$ channel blockers. Under these conditions, bupivacaine and quinine decreased transient outward currents, mimicking the effect of 4-aminopyridine (4-AP; 4 mM) (supplemental Fig. 6, available at www.jneurosci.org as supplemental material). Hence, to isolate putative quinine- and bupivacaine-sensitive K$_{2P}$ currents in hippocampal astrocytes, coapplication of Ba^{2+} and 4-AP is necessary.

In the presence of Ba^{2+} (100 μM) and 4-AP (4 mM), application of quinine (200 μM) decreased the membrane conductance by 61 ± 10% (+20 mV) and 31 ± 10% (−130 mV; $n = 9$), respectively (Fig. 9B1–B3). Quinine caused an additional depolarization, shifting V_R from −55.2 ± 9.8 mV (in the presence of Ba^{2+} and 4-AP) to −44.4 ± 12.2 mV ($n = 9$). The quinine sensitive current showed outward rectification, as predicted for open channels by the Goldman-Hodgkin-Katz equation. In the same cells, E_{rev} of Ba^{2+}-sensitive currents mediated by Kir4.1 was −74.7 ± 6.8 mV (RI, 0.76 ± 0.16; $n = 9$), whereas quinine-

sensitive, presumed K_{2P} channel-mediated currents (i.e., recorded in the presence of Ba^{2+} and 4-AP) reversed at -66.8 ± 12.9 mV. The latter displayed pronounced outward rectification (RI, 2.28 ± 1.50; $n = 9$). Bupivacaine (200 μM), in the presence of Ba^{2+} and 4-AP, neither changed V_R nor membrane conductance ($n = 7$) (Fig. 9*B4*).

We determined the relative reduction of membrane conductance when consecutively applying Ba^{2+}, 4-AP, and quinine to the same cell. At $+20$ mV, Ba^{2+} decreased the membrane conductance by $56.9 \pm 16.1\%$ (data taken 50 ms after stimulus onset). The addition of 4-AP to the Ba^{2+}-containing solution led to an additional decrease of ~15.9% (total decrease of $72.8 \pm 6.3\%$), and quinine blocked another 16.2% (total decrease of $89 \pm 4.5\%$; $n = 9$; residual membrane conductance, $11 \pm 4.5\%$). At -130 mV, Ba^{2+} decreased the conductance by $80.7 \pm 11.6\%$. 4-AP had almost no effect (additional decrease of 0.7%), whereas addition of quinine led to a total decrease of $89.1 \pm 5.5\%$ (residual membrane conductance, $10.9 \pm 5.5\%$) (Fig. 9*D*). To test for the K^+ selectivity of quinine-sensitive, presumed K_{2P} channels, the extracellular K^+ concentration was increased to 50 mM. In the presence of Ba^{2+} and 4-AP, quinine-sensitive currents reversed at -22.9 ± 1.1 mV ($n = 5$) (i.e., close to the K^+ equilibrium potential; -24.1 mV). The *I/V* relationship of the corresponding conductance was almost linear (RI, 1.12 ± 0.13).

The shape of the *I/V* relationship of quinine-sensitive currents, the insensitivity of membrane currents to acid pH (compare supplemental Fig. 2, available at www.jneurosci.org as supplemental material), and the small effects of bupivacaine suggested expression of TREK family K_{2P} channels (Goldstein et al., 2001) in hippocampal astrocytes. TREK-mediated currents are potentiated by polyunsaturated fatty acids such as AA and by volatile anesthetics (e.g., halothane) (for review, see Honoré, 2007). To substantiate the hypothesis that the cells under study express TREK channels, AA (10 μM) was applied to isolated astrocytes, subsequent to adding Ba^{2+} (100 μM), 4-AP (4 mM), and tetraethylammonium (TEA) (10 mM) to the bath. Application of AA (duration $\leq$2 min) increased the membrane currents to $172 \pm 38\%$ ($+20$ mV; range, 125–250%; $n = 8$) (Fig. 10*A,B*). AA increased outwardly rectifying currents (RI, 1.78 ± 1.00; $[K^+]_o = 5$ mM) with $E_{rev} = -66.7 \pm 16.5$ mV ($n = 8$). In 50 mM K^+-containing bath solution, E_{rev} shifted to -25.3 ± 3.2 mV (RI, 1.29 ± 0.23; $n = 5$) (Fig. 10*C–E*). The potentiating effect of AA was reversible and blocked by quinine (200 μM; data not shown). Halothane (5 mM, 1 min; in the presence of Ba^{2+}, 4-AP, and TEA) also exerted a potentiating effect. Membrane currents increased to 142 ± 79 and $149 \pm 58\%$ at $+20$ and -130 mV, respectively ($n = 5$; data not shown). Together, these data suggested that astrocytes in the hippocampus express K_{2P} family members, presumably TREK1 and/or TREK2.

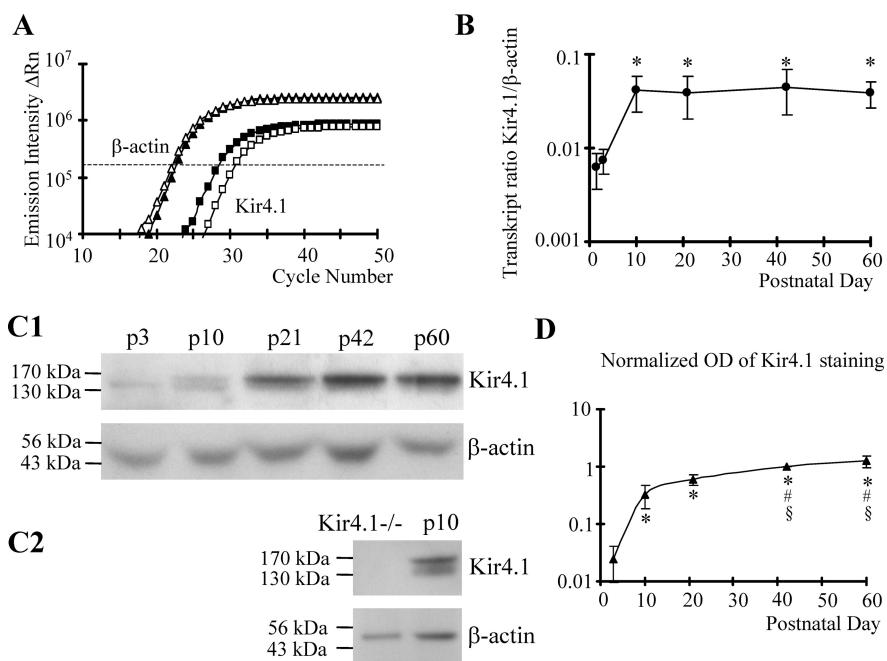To further corroborate this hypothesis and identify K_{2P} sub-

Figure 5. Developmental regulation of Kir4.1 mRNA and protein in the CA1 region. *A*, Amplification plots for Kir4.1 (squares) and β-actin (triangles) of two mRNA samples were obtained using real-time sqRT-PCR. mRNA was analyzed from mice at P3 (open symbols) and P21 (filled symbols). The difference in threshold cycles (ΔRn; taken at the dashed line) at P3 was larger than that at P21. *B*, The corresponding gene expression ratio, Kir4.1/β-actin, was determined according to Equation 5 and blotted against age. Mean and SD were obtained at P1 and P3 (12 samples each) and at P10, P21, P42, and P60 (10 samples each). The increase in Kir4.1 expression between P1 or P3 and the other time points was significant (*). *C1*, Roentgen films of Western blot analysis of Kir4.1 tetramers (~160 kDa) and β-actin (42 kDa). Protein content of lysates prepared from whole hippocampi was analyzed at the ages indicated. The β-actin signal served as a loading control (60 μg of protein each). *C2*, Absence of Kir4.1 protein in Kir4.1$-/-$ mice compared with wild type (P10; β-actin served as a control). *D*, The optical density (OD) of Kir4.1 tetramer signals was corrected with respect to β-actin for each sample. Subsequently, OD values were normalized to Kir4.1 at P42. The plot shows mean values of six mice. Differences between P3 and P10–P60 (*), P10 and P42–P60 (#), and P21 and P42–P60 ($\S$) were statistically significant.

units expressed by hippocampal astrocytes, postrecording multiplex single-cell RT-PCR was performed. All astrocytes tested expressed Kir4.1 ($n = 43$). Coexpression of subunits of the TREK family together with Kir4.1 was tested in 28 cells. TREK1 was found in 61% ($n = 17$ of 28) of the astrocytes, whereas 23% (3 of 13) of the Kir4.1-positive cells contained mRNA encoding TREK2. Some cells ($n = 2$ of 13) coexpressed TREK1, TREK2, and Kir4.1. In addition, a majority (67%) of Kir4.1-positive astrocytes contained TWIK1 transcripts ($n = 14$ of 21). In contrast, transcripts for TRAAK were never found (0 of 9) (Fig. 10*F*). Hippocampal astrocytes from Kir4.1$-/-$ mice also expressed TWIK1 and TREK1 transcripts (64% each; $n = 11$) and displayed AA (10 μM)-sensitive currents (data not shown).

Discussion

Despite the fact that astrocytes are increasingly recognized as communication partners of neurons (Volterra and Meldolesi, 2005; Haydon and Carmignoto, 2006), the intrinsic biophysical properties of these cells are poorly understood. Thus, although it is known for many years that the astrocytic membrane *in situ* is dominated by prominent resting currents (Steinhäuser et al., 1992), the composition of ion channels mediating this "passive" current phenotype is not well defined. Part of this ignorance is attributable to the fact that astrocytes are abundantly coupled, giving rise to a significant intercellular conductance (Blomstrand et al., 2004; Wallraff et al., 2006) impeding quantitative analyses of intrinsic astrocytic currents. The matter is further complicated since astrocytes in different brain regions display variable func-
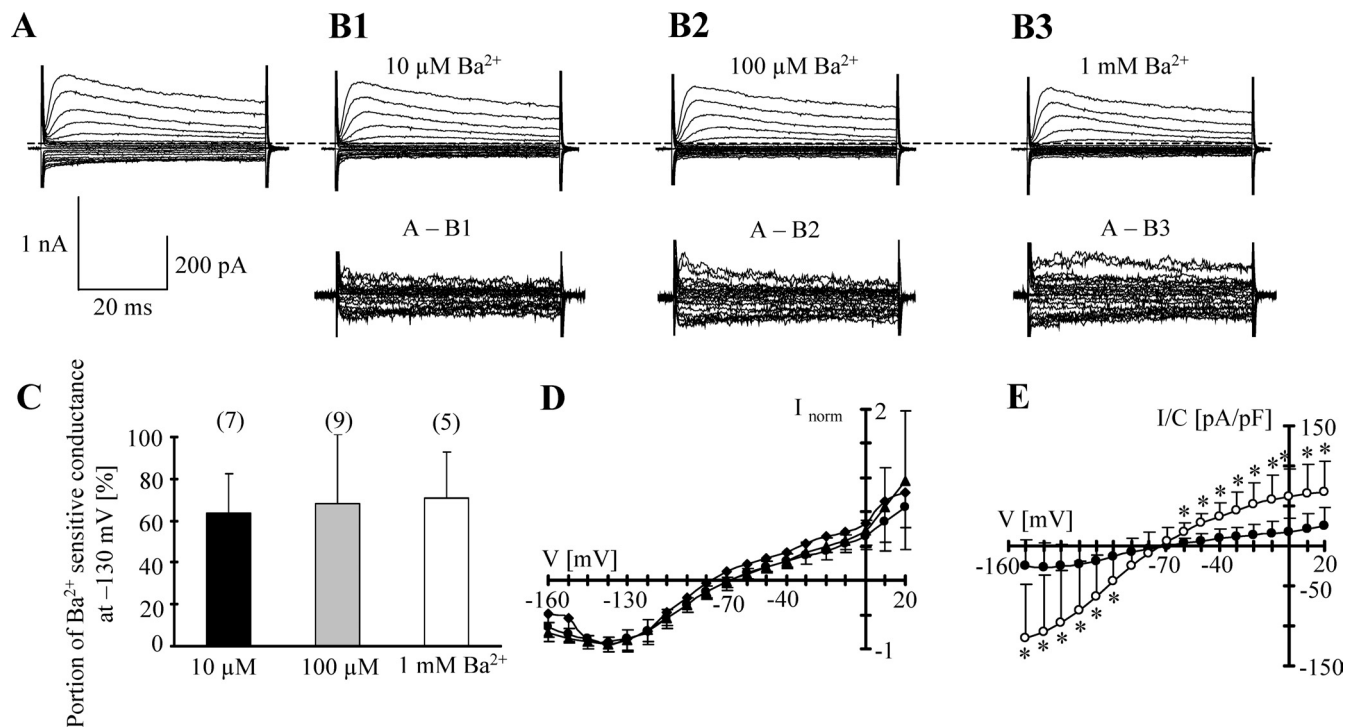
Figure 6. Ba^{2+} sensitivity of membrane currents of freshly isolated astrocytes at P1. **A**, Membrane currents were evoked as described in Figure 1. **B1–B3**, Ba^{2+}-sensitive currents were isolated by subtracting current families obtained in Ba^{2+} from those before Ba^{2+} application at corresponding voltages (bottom; scale bar, 200 pA). **C**, Membrane conductance in control and Ba^{2+} solutions was determined at −130 mV according to Equation 1, and Ba^{2+}-sensitive fractions were determined at different concentrations of the blocker (cell numbers are in parentheses). **D**, I/V relationships of Ba^{2+}-sensitive currents in 0.01 mM Ba^{2+} (diamonds; $n = 8$), 0.1 mM Ba^{2+} (circles; $n = 9$), and 1 mM Ba^{2+} (triangles; $n = 5$). Data were normalized to respective maximum inward currents. **E**, Comparison of Ba^{2+}-sensitive current densities (100 μM) at P9 ($n = 9$; taken from Fig. 2; open circles) and P1 ($n = 9$; filled circles). Current densities of the two curves differed significantly between −150 and −100 mV and between −60 and +20 mV (*). Data in **C–E** are given as mean ± SD.
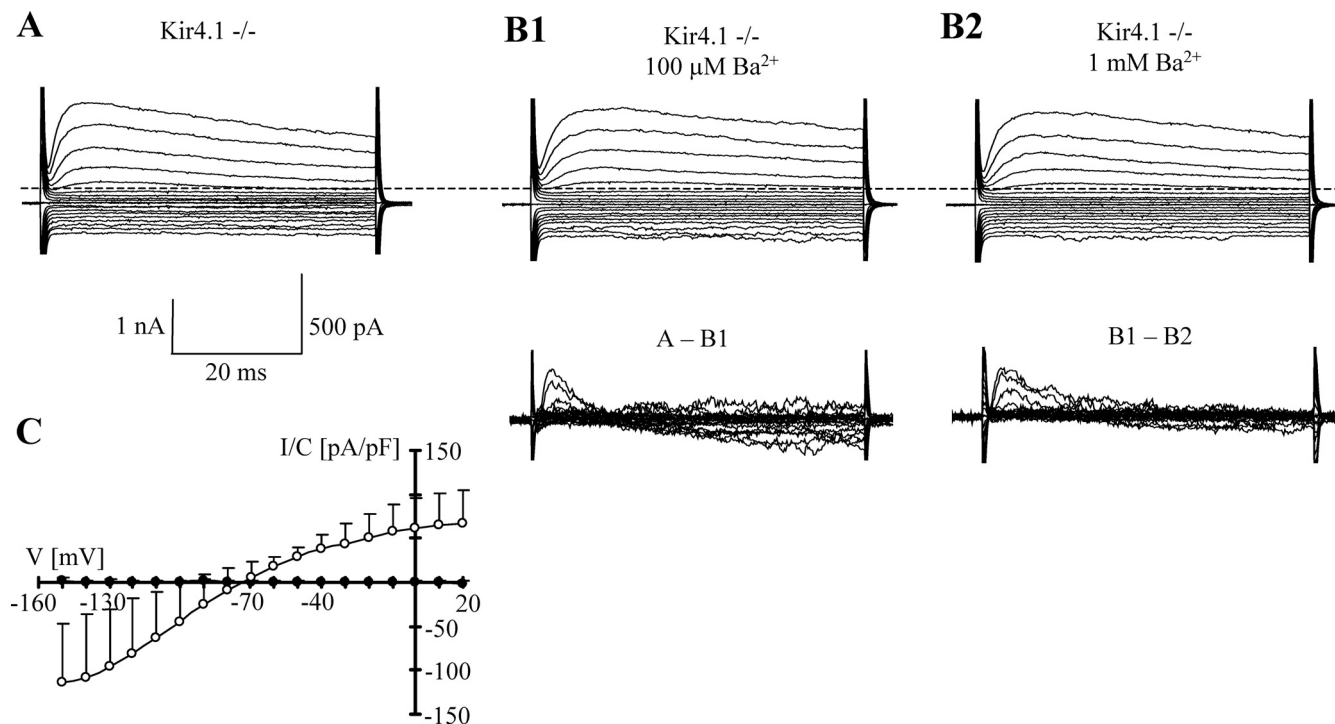

Figure 7. Lack of Ba^{2+}-sensitive currents in astrocytes freshly isolated from Kir4.1−/−;Tg(hGFAP/EGFP) mice (P9). **A**, Membrane currents were evoked as described in Figure 1. **B1**, **B2**, Ba^{2+} did not affect inward currents. Bottom panels show the Ba^{2+}-sensitive components at higher resolution (scale bar, 500 pA). **C**, The mean I/V relationship of Ba^{2+} (100 μM)-sensitive current densities of 10 astrocytes obtained from the CA1 region of Kir4.1−/−;Tg(hGFAP/EGFP) mice (filled circles; data taken after 50 ms). For comparison, Ba^{2+} (100 μM)-sensitive currents at P9 ($n = 9$; open circles; taken from Fig. 2) were depicted.

tional properties (Clark and Barbour, 1997; Matthias et al., 2003; Lalo et al., 2006, 2008; Jabs et al., 2007). Using freshly isolated cells to improve space-clamp conditions, we show here that the majority of inward currents in hippocampal astrocytes are mediated by Kir4.1 and that these cells also express functional K_{2P} channels.

Developmental and spatial regulation of Kir4.1

Single-cell transcript analysis and protein measurements in the CA1 region indicated strong upregulation of Kir4.1 during early postnatal development, which was accompanied by increasing Ba^{2+}-sensitive inward currents. Notably, in perinatal astrocytes, the small Kir currents were sufficient to stabilize V_R close to E_K, which is different to retinal Müller cells (Bringmann et al., 1999, 2000).

Beyond P10, Kir4.1 mRNA in the hippocampus was higher in stratum lacunosum-moleculare compared with the radiatum. The radiatum harbors most of the CA1 excitatory input, whereas only 20% of pyramidal cell synapses are located in the lacunosum-moleculare (Megias et al., 2001). At the same time, the lacunosum-moleculare is the region with the highest density of perfused microvessels in the hippocampus (Gerhart et al., 1991; Shimada et al., 1992). Kir4.1 is highly expressed around synapses and blood vessels (Higashi et al., 2001; Hibino et al., 2004), and colocalized AQP4 and Kir4.1 channels in astrocytic endfeet touching microvessels mediate coupled transport of K^+ and water (Nagelhus et al., 2004; Dibaj et al., 2007). The finding of a concerted developmental increase of AQP4 and Kir4.1 in astrocytes and Müller cells further supports their critical involvement in brain water regulation, K^+ homeostasis, and volume regulation (Wen et al., 1999; Wurm et al., 2006). Accordingly, lysis of the perivascular AQP4/Kir4.1 complex perturbs K^+ homeostasis and promotes epilepsy (Eid et al., 2005).

The localization of Kir4.1 at processes wrapping synapses and blood vessels led to the concept of glial K^+ spatial buffering (Orkand, 1986). This concept has been confirmed in the retina (K^+ siphoning) (Newman and Reichenbach, 1996), whereas knowledge of other brain areas remained limited (Holthoff and Witte, 2000). A recent study, using transgenic mice with genetic deletion of Cx30 and Cx43 in astrocytes, provided evidence that spatial K^+ buffering is also operative in gray matter (Wallraff et al., 2006). Presumably, astrocytes in the radiatum use indirect coupling to evacuate K^+ into the microvasculature.

Pathological impact of Kir4.1 regulation in astrocytes

In the present study, the pivotal role of Kir4.1 channels in constituting the membrane conductance of developing astrocytes in the hippocampus was confirmed using constitutive Kir4.1−/− mice. Astrocytes of these mice lacked Ba^{2+}-sensitive currents and dis-
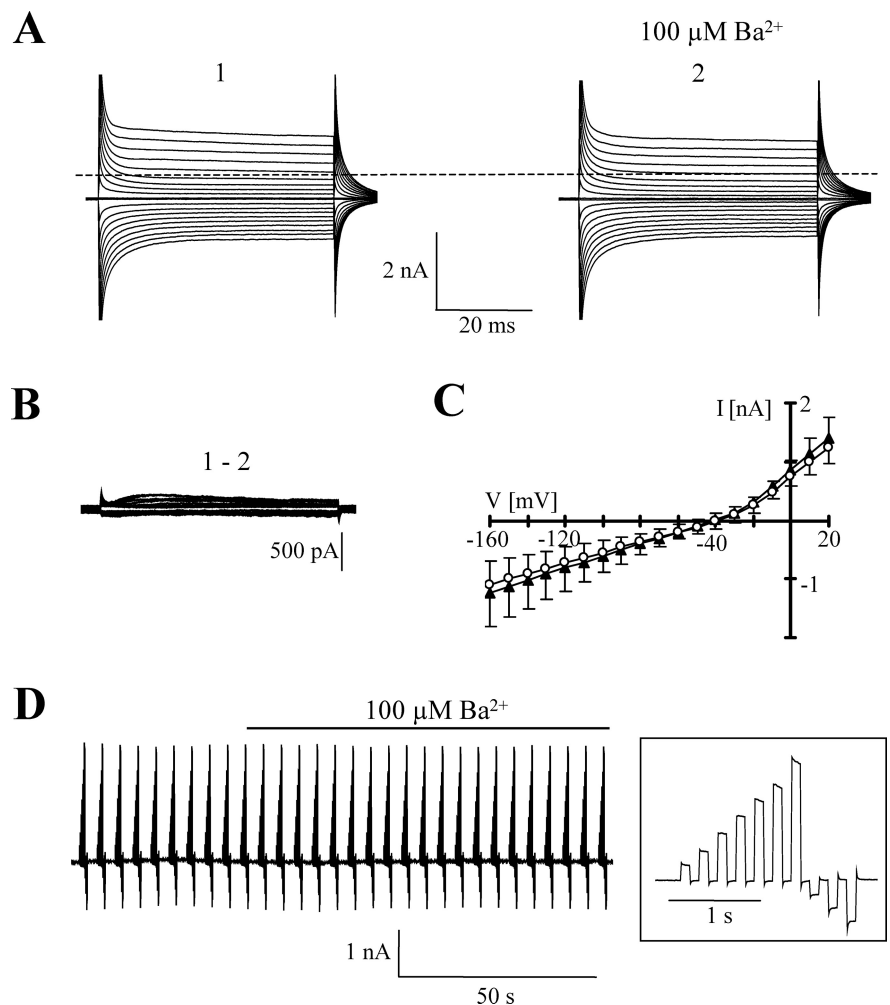

Figure 8. Astrocytes in Kir4.1−/−;Tg(hGFAP/EGFP) mice (P9) *in situ* lack Ba^{2+}-sensitive currents. **A**, Membrane currents before (left) and in the presence of (right) Ba^{2+} (100 μM) were elicited as described in Figure 1. **B**, The Ba^{2+}-sensitive component was isolated through a subtraction protocol. **C**, Mean (9 cells) *I/V* relationships were determined before (filled triangles) and during (open circles) application of Ba^{2+} (100 μM). **D**, The membrane was repetitively clamped between −160 and +100 mV for 100 ms, separated by 100 ms (holding potential, −70 mV; see inset), and 100 μM Ba^{2+} was added via the bath as indicated, confirming that Ba^{2+} had no effect on current amplitudes.

played depolarized V_R. Conditional knock-out of Kir4.1 also led to astrocyte depolarization, inhibition of K^+ and glutamate uptake, and enhanced short-term synaptic potentiation (Djukic et al., 2007).

Astrocyte dysfunction is increasingly recognized as an important factor in the pathogenesis of neurological disorders (Seifert et al., 2006). Reduced astroglial Kir currents were observed under various pathological conditions [e.g., after entorhinal cortex lesion (Schröder et al., 1999), cortical dysplasia (Bordey et al., 2001), and traumatic and ischemic brain injury (D'Ambrosio et al., 1999; Köller et al., 2000); in Cu/Zn SOD (superoxide dismutase)-1 mutant mice, a model for familial amyotrophic lateral sclerosis (Kaiser et al., 2006); and in neurosurgical specimens from epilepsy patients (Bordey and Sontheimer, 1998; Hinterkeuser et al., 2000)]. Impaired function of glutamate uptake may add to pathological effects of Kir loss in astrocytes (Kucheryavykh et al., 2007). Notably, transient opening of the blood–brain barrier is sufficient for focal epileptogenesis, probably because of astroglial albumin uptake triggering downregulation of Kir4.1 (Ivens et al., 2007).

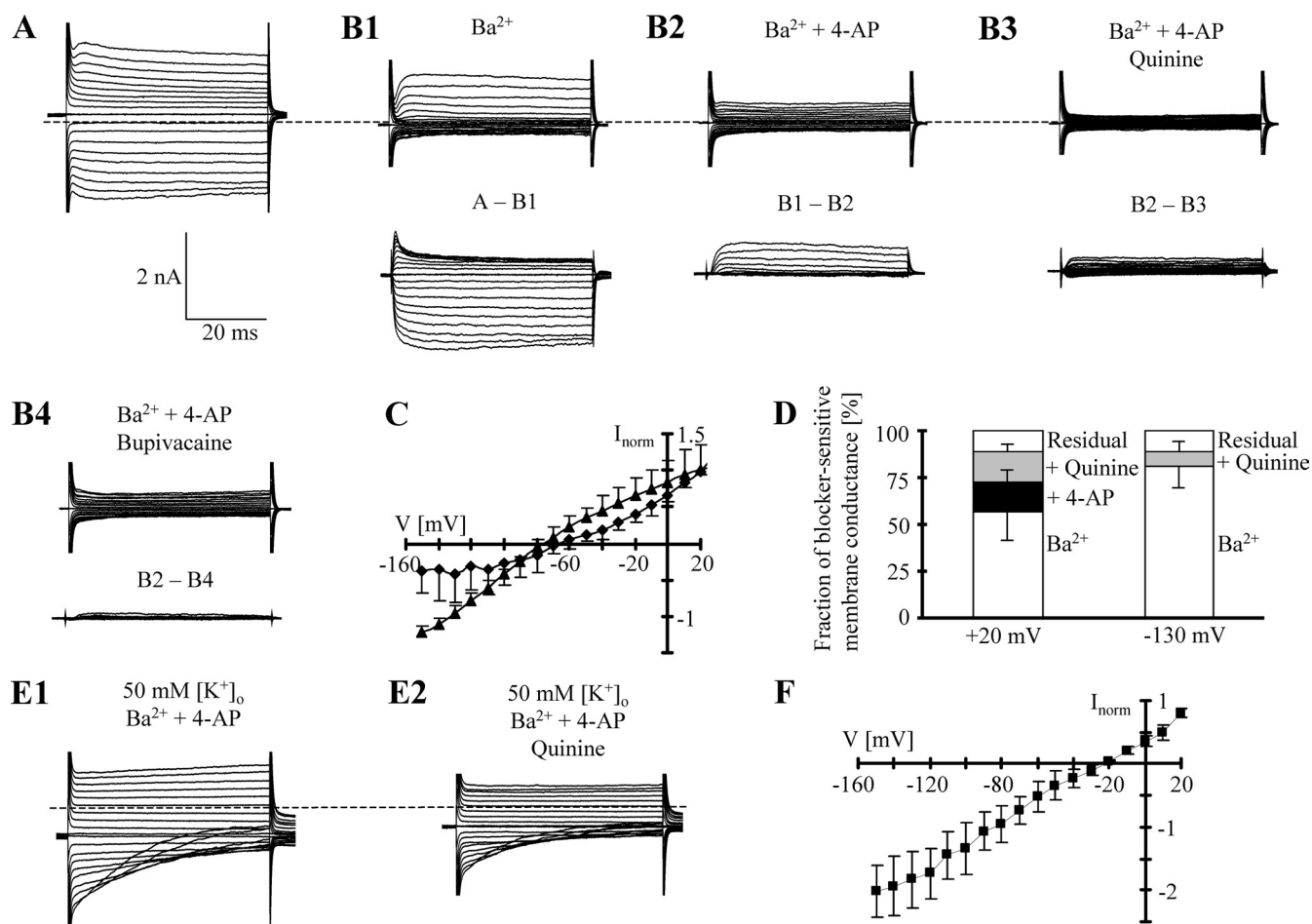Astrocytic Kir4.1 channels become Ca^{2+} permeable at low

Figure 9. Isolation of quinine-sensitive currents in isolated astrocytes. **A**, Currents were activated between -150 and $+30$ mV (holding potential, -60 mV; $V_R = -68$ mV). The dashed line indicates zero current. **B1–B3**, Ba^{2+} (100 μM), 4-AP (4 mM), and quinine (200 μM) were consecutively applied to the same cell. Bottom panels show the Ba^{2+}-sensitive (**B1**), 4-AP-sensitive (**B2**), and quinine-sensitive (**B3**) currents. **B4**, After washout of quinine, bupivacaine (200 μM) was applied to the same cell, indicating that bupivacaine and 4-AP blocked almost the same currents (**B2–B4**). **C**, The mean I/V relationship of Ba^{2+}-sensitive (triangles) and quinine-sensitive (diamonds) currents. Data were taken 50 ms after stimulus onset and normalized to maximum inward (Ba^{2+}) or outward current amplitudes (quinine) obtained in each individual cell ($n = 9$). Note the weak inward rectification of Ba^{2+}-sensitive currents while quinine currents were outwardly rectifying. **D**, Estimation of the relative fraction of currents sensitive to Ba^{2+}, Ba^{2+} plus 4-AP, and Ba^{2+} plus 4-AP plus quinine. Membrane conductance was determined at $+20$ and -130 mV and averaged ($n = 9$; mean $\pm$ SD). **E1**, **E2**, In high-[K$^+$]$_o$ solution supplemented with Ba^{2+} (100 μM) and 4-AP (4 mM), quinine (200 μM) decreased membrane currents. **F**, Mean I/V relationship of quinine-sensitive currents (solutions as in **E**), normalized to maximum current in each cell ($n = 5$). Note that in high-K$^+$ solution, quinine-sensitive currents lost outward rectification and reversed close to E_K (-24.1 mV).

extracellular K$^+$ concentrations. Thus, under conditions of local K$^+$ undershoot attributable to enhanced Na$^+$/K$^+$ ATPase activity, Kir4.1 channels potentially trigger Ca^{2+} oscillations and gliotransmitter release, which might exacerbate pathological conditions (Dallwig et al., 2000; Hartel et al., 2007).

Passive current pattern of astrocytes
Based on initial recordings in acute hippocampal brain slices, glial cells with predominating passive and "complex" current patterns have been distinguished (Steinhäuser et al., 1994), and later work has established that passive cells represent *bona fide* astrocytes whereas complex cells constitute a different cell type (termed GluR cells or NG2 glia) (Matthias et al., 2003; Wigley et al., 2007). However, it is still unclear which ion channel(s), in addition to Kir4.1, underlies the passive currents of astrocytes in the hippocampus. Currents through gap junctions contribute to the overall conductance, but even after genetical deletion of coupling the passive current phenotype remained (Wallraff et al., 2006).

Interestingly, whole-cell recordings from freshly isolated as-

trocytes often disclosed time- and voltage-dependent currents (see also Matthias et al., 2003), which were obviously masked by the much larger passive currents activated in slice recordings. Perinatally, however, even slice recordings frequently reveal complex current patterns in astrocytes (data not shown). Accordingly, early in development (i.e., before P12), the whole-cell current pattern cannot be used as a reliable criterion to distinguish astrocytes from GluR cells or NG2 glia. Similar observations have been made in rat hippocampus (Zhou et al., 2006).

Expression of K$_{2P}$ channels by hippocampal astrocytes
It has been suggested that K$_{2P}$ channels mediate part of the passive astroglial membrane conductance. Astrocytes of hippocampus and cerebellum express TASK1 protein (Kindler et al., 2000; Millar et al., 2000; Kanjhan et al., 2004; Rusznak et al., 2004; Kim et al., 2007), but so far evidence of functional expression of acid- and bupivacaine-sensitive TASK channels in these cells is lacking. The present study also failed at finding effects of bupivacaine after inhibiting Kir- and 4-AP-sensitive voltage-gated currents. Moreover, acid pH had only small effects on astrocyte currents, and the
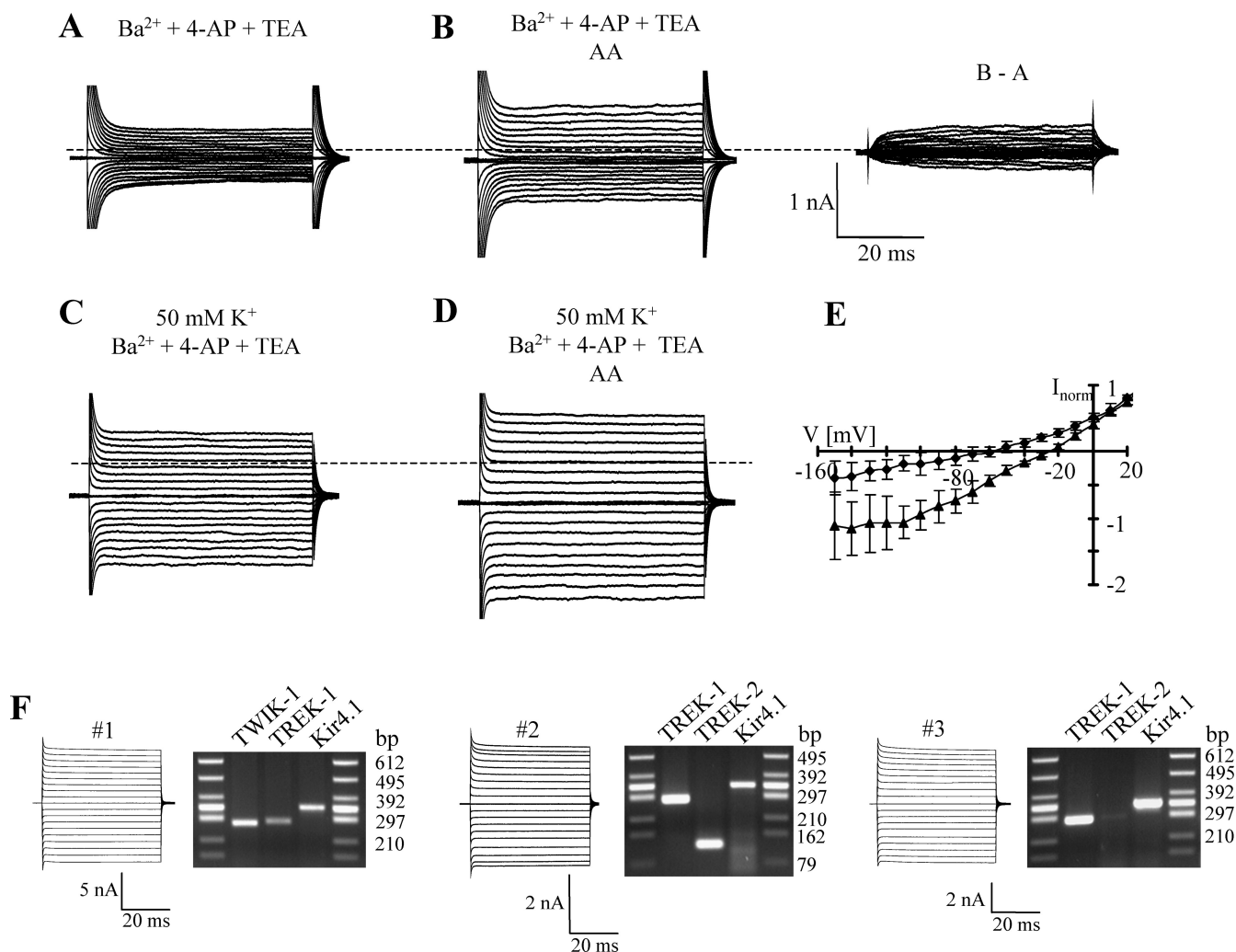
Figure 10. Hippocampal astrocytes express functional TREK channels. **A**, **B**, In the presence of Ba^{2+} (100 μM), 4-AP (4 mM), and TEA (10 mM), AA (10 μM; 1 min) increased membrane currents (stimulus protocol as in Fig. 9; dotted lines indicate zero current at -70 mV). AA-sensitive currents are shown to the right (B $-$ A). **C**, **D**, The blockers used in **A** and **B** were applied in high-$[K^+]_o$ solution. AA (10 μM) led to a current increase. **E**, Mean *I/V* relationships of AA-induced currents (diamonds, 5 mM $[K^+]_o$, $n = 8$; triangles, 50 mM $[K^+]_o$, $n = 5$). Data were taken 50 ms after stimulus onset. **F**, Analysis of Kir and K_{2P} transcripts in single astrocytes. After recording (-160 to $+20$ mV; holding potential, -70 mV), the cytoplasm was harvested, and multiplex RT-PCR was performed. Agarose gels show PCR products for K_{2P} and Kir4.1 channels. The expected product lengths were 338 bp for Kir4.1, 282 bp for TREK1, 126 bp for TREK2, and 272 bp for TWIK1.

I/V relationship of this pH-sensitive component rather indicated weak pH dependence of Kir channels. The conclusion that hippocampal astrocytes lack TASK channels is in line with Päsler et al. (2007), who did not observe bupivacaine-sensitive K^+ uptake. Bupivacaine-sensitive, presumed TASK channel-mediated currents were described in Müller cells (Skatchkov et al., 2006).

In the present study, quinine-sensitive K^+ currents were identified that displayed outwardly rectifying *I/V* relationships as predicted for open channels from the Goldman-Hodgkin-Katz relationship. In the presence of Ba^{2+}, TEA, and 4-AP (i.e., blockers of Kir and voltage-gated K^+ channels), AA and halothane reversibly increased presumed K_{2P} currents. Potentiation was blocked by quinine. In high K^+ solution, E_{rev} of AA$-$ or halothane-sensitive currents shifted as expected for K^+-permeable channels. Together, this indicated functional expression of TREK-like channels (Patel et al., 1998). Previous work using cultured astrocytes reported TREK-like currents that were sensitive to quinine and polyunsaturated fatty acids (Gnatenco et al., 2002; Ferroni et al., 2003). To further confirm expression of K_{2P} channels in acute hippocampal astrocytes, single-cell RT-PCR was performed. Using primers recognizing Kir4.1 together with K_{2P} subunits, we

found that most cells expressed TREK whereas TRAAK was lacking, which was consistent with our functional analyses. In addition, many astrocytes contained mRNAs for TWIK1. These channels are highly sensitive to Ba^{2+} ($IC_{50} = \sim100$ μM) and quinine ($IC_{50} = \sim50$ μM) (Lesage et al., 1996). However, since TWIK1 channels show inward rectification and because no Ba^{2+} sensitivity was observed in astrocytes from Kir4.1$-/-$ mice (although astrocytes from these mice displayed unchanged TWIK1 transcript expression), it is unlikely that TWIK1 channels substantially contribute to the current pattern of astrocytes in the CA1 region of the hippocampus.

In conclusion, our data suggest that astrocytes express K_{2P} channels of the TREK family. Assuming that they are expressed at distant processes or endfeet and subject to modulation by endogenously released AA, TREK channels might serve the fine tuning of K^+ homeostasis at the neurovascular interface (Mulligan and MacVicar, 2004). The present study suggests that the apparently ohmic whole-cell current pattern of astrocytes results from the superposition of several components, including Kir currents, 4-AP-sensitive voltage-gated currents, and currents through K_{2P} channels. Using independent methodological approaches, our

findings substantiate that Kir4.1 constitutes a pivotal subunit mediating inward currents in hippocampal astrocytes. In addition, it provides the first quantitative comparative evaluation of Kir4.1 expression in the CA1 subfield and its regulation during postnatal development. Improved knowledge of basic astrocyte physiology is necessary for a better understanding of the neuron–glia cross talk in the normal and diseased brain.

References

Blomstrand F, Venance L, Siren AL, Ezan P, Hanse E, Glowinski J, Ehrenreich H, Giaume C (2004) Endothelins regulate astrocyte gap junctions in rat hippocampal slices. Eur J Neurosci 19:1005–1015.

Bordey A, Sontheimer H (1998) Properties of human glial cells associated with epileptic seizure foci. Epilepsy Res 32:286–303.

Bordey A, Lyons SA, Hablitz JJ, Sontheimer H (2001) Electrophysiological characteristics of reactive astrocytes in experimental cortical dysplasia. J Neurophysiol 85:1719–1731.

Bringmann A, Biedermann B, Reichenbach A (1999) Expression of potassium channels during postnatal differentiation of rabbit Muller glial cells. Eur J Neurosci 11:2883–2896.

Bringmann A, Francke M, Pannicke T, Biedermann B, Kodal H, Faude F, Reichelt W, Reichenbach A (2000) Role of glial K$^+$ channels in ontogeny and gliosis: a hypothesis based upon studies on Muller cells. Glia 29:35–44.

Casamassima M, D'Adamo MC, Pessia M, Tucker SJ (2003) Identification of a heteromeric interaction that influences the rectification, gating, and pH sensitivity of Kir4.1/Kir5.1 potassium channels. J Biol Chem 278:43533–43540.

Clark BA, Barbour B (1997) Currents evoked in Bergmann glial cells by parallel fibre stimulation in rat cerebellar slices. J Physiol 502:335–350.

Dallwig R, Vitten H, Deitmer JW (2000) A novel barium-sensitive calcium influx into rat astrocytes at low external potassium. Cell Calcium 28:247–259.

D'Ambrosio R, Maris DO, Grady MS, Winn HR, Janigro D (1999) Impaired K$^+$ homeostasis and altered electrophysiological properties of posttraumatic hippocampal glia. J Neurosci 19:8152–8162.

Dibaj P, Kaiser M, Hirrlinger J, Kirchhoff F, Neusch C (2007) Kir4.1 channels regulate swelling of astroglial processes in experimental spinal cord edema. J Neurochem 103:2620–2628.

Djukic B, Casper KB, Philpot BD, Chin LS, McCarthy KD (2007) Conditional knock-out of Kir4.1 leads to glial membrane depolarization, inhibition of potassium and glutamate uptake, and enhanced short-term synaptic potentiation. J Neurosci 27:11354–11365.

Eid T, Lee TS, Thomas MJ, Amiry-Moghaddam M, Bjornsen LP, Spencer DD, Agre P, Ottersen OP, De Lanerolle NC (2005) Loss of perivascular aquaporin 4 may underlie deficient water and K+ homeostasis in the human epileptogenic hippocampus. Proc Natl Acad Sci U S A 102:1193–1198.

Ferroni S, Valente P, Caprini M, Nobile M, Schubert P, Rapisarda C (2003) Arachidonic acid activates an open rectifier potassium channel in cultured rat cortical astrocytes. J Neurosci Res 72:363–372.

Gerhart DZ, Djuricic B, Drewes LR (1991) Quantitative immunocytochemistry (image analysis) of glucose transporters in the normal and postischemic rodent hippocampus. J Cereb Blood Flow Metab 11:440–448.

Gnatenco C, Han J, Snyder AK, Kim D (2002) Functional expression of TREK-2 K(+) channel in cultured rat brain astrocytes. Brain Res 931:56–67.

Goldstein SA, Bockenhauer D, O'Kelly I, Zilberberg N (2001) Potassium leak channels and the KCNK family of two-P-domain subunits. Nat Rev Neurosci 2:175–184.

Hartel K, Singaravelu K, Kaiser M, Neusch C, Hulsmann S, Deitmer JW (2007) Calcium influx mediated by the inwardly rectifying K+ channel Kir4.1 (KCNJ10) at low external K+ concentration. Cell Calcium 42:271–280.

Haydon PG, Carmignoto G (2006) Astrocyte control of synaptic transmission and neurovascular coupling. Physiol Rev 86:1009–1031.

Heinemann U, Gabriel S, Jauch R, Schulze K, Kivi A, Eilers A, Kovacs R, Lehmann TN (2000) Alterations of glial cell function in temporal lobe epilepsy. Epilepsia 41 [Suppl 6]:S185–S189.

Hibino H, Fujita A, Iwai K, Yamada M, Kurachi Y (2004) Differential assembly of inwardly rectifying K+ channel subunits, Kir4.1 and Kir5.1, in brain astrocytes. J Biol Chem 279:44065–44073.

Higashi K, Fujita A, Inanobe A, Tanemoto M, Doi K, Kubo T, Kurachi Y (2001) An inwardly rectifying K(+) channel, Kir4.1, expressed in astrocytes surrounds synapses and blood vessels in brain. Am J Physiol Cell Physiol 281:C922–C931.

Hinterkeuser S, Schröder W, Hager G, Seifert G, Blümcke I, Elger CE, Schramm J, Steinhäuser C (2000) Astrocytes in the hippocampus of patients with temporal lobe epilepsy display changes in potassium conductances. Eur J Neurosci 12:2087–2096.

Holthoff K, Witte OW (2000) Directed spatial potassium redistribution in rat neocortex. Glia 29:288–292.

Honoré E (2007) The neuronal background K2P channels: focus on TREK1. Nat Rev Neurosci 8:251–261.

Ishii M, Horio Y, Tada Y, Hibino H, Inanobe A, Ito M, Yamada M, Gotow T, Uchiyama Y, Kurachi Y (1997) Expression and clustered distribution of an inwardly rectifying potassium channel, KAB-2/Kir4.1, on mammalian retinal Muller cell membrane: their regulation by insulin and laminin signals. J Neurosci 17:7725–7735.

Ishii M, Fujita A, Iwai K, Kusaka S, Higashi K, Inanobe A, Hibino H, Kurachi Y (2003) Differential expression and distribution of Kir5.1 and Kir4.1 inwardly rectifying K+ channels in retina. Am J Physiol Cell Physiol 285:C260–C267.

Ivens S, Kaufer D, Flores LP, Bechmann I, Zumsteg D, Tomkins O, Seiffert E, Heinemann U, Friedman A (2007) TGF-beta receptor-mediated albumin uptake into astrocytes is involved in neocortical epileptogenesis. Brain 130:535–547.

Jabs R, Pivneva T, Huttmann K, Wyczynski A, Nolte C, Kettenmann H, Steinhauser C (2005) Synaptic transmission onto hippocampal glial cells with hGFAP promoter activity. J Cell Sci 118:3791–3803.

Jabs R, Matthias K, Grote A, Grauer M, Seifert G, Steinhauser C (2007) Lack of P2X receptor mediated currents in astrocytes and GluR type glial cells of the hippocampal CA1 region. Glia 55:1648–1655.

Kaiser M, Maletzki I, Hulsmann S, Holtmann B, Schulz-Schaeffer W, Kirchhoff F, Bahr M, Neusch C (2006) Progressive loss of a glial potassium channel (KCNJ10) in the spinal cord of the SOD1 (G93A) transgenic mouse model of amyotrophic lateral sclerosis. J Neurochem 99:900–912.

Kanjhan R, Anselme AM, Noakes PG, Bellingham MC (2004) Postnatal changes in TASK-1 and TREK-1 expression in rat brain stem and cerebellum. Neuroreport 15:1321–1324.

Kim DS, Kim JE, Kwak SE, Choi HC, Song HK, Kimg YI, Choi SY, Kang TC (2007) Up-regulated astroglial TWIK-related acid-sensitive K(+) channel-1 (TASK-1) in the hippocampus of seizure-sensitive gerbils: a target of anti-epileptic drugs. Brain Res 1185:346–358.

Kindler CH, Pietruck C, Yost CS, Sampson ER, Gray AT (2000) Localization of the tandem pore domain K$^+$ channel TASK-1 in the rat central nervous system. Mol Brain Res 80:99–108.

Kofuji P, Newman EA (2004) Potassium buffering in the central nervous system. Neuroscience 129:1045–1056.

Kofuji P, Ceelen P, Zahs KR, Surbeck LW, Lester HA, Newman EA (2000) Genetic inactivation of an inwardly rectifying potassium channel (Kir4.1 subunit) in mice: phenotypic impact in retina. J Neurosci 20:5733–5740.

Köller H, Schroeter M, Jander S, Stoll G, Siebler M (2000) Time course of inwardly rectifying K$^+$ current reduction in glial cells surrounding ischemic brain lesions. Brain Res 872:194–198.

Kucheryavykh YV, Kucheryavykh LY, Nichols CG, Maldonado HM, Baksi K, Reichenbach A, Skatchkov SN, Eaton MJ (2007) Downregulation of Kir4.1 inward rectifying potassium channel subunits by RNAi impairs potassium transfer and glutamate uptake by cultured cortical astrocytes. Glia 55:274–281.

Lalo U, Pankratov Y, Kirchhoff F, North RA, Verkhratsky A (2006) NMDA receptors mediate neuron-to-glia signaling in mouse cortical astrocytes. J Neurosci 26:2673–2683.

Lalo U, Pankratov Y, Wichert SP, Rossner MJ, North RA, Kirchhoff F, Verkhratsky A (2008) P2X1 and P2X5 subunits form the functional P2X receptor in mouse cortical astrocytes. J Neurosci 28:5473–5480.

Lesage F, Lazdunski M (2000) Molecular and functional properties of two-pore-domain potassium channels. Am J Physiol Renal Physiol 279:F793–F801.

Lesage F, Reyes R, Fink M, Duprat F, Guillemare E, Lazdunski M (1996) Dimerization of TWIK-1 K$^+$ channel subunits via a disulfide bridge. EMBO J 15:6400–6407.

Li LY, Head V, Timpe LC (2001) Identification of all inward rectifier potassium channel gene expressed in mouse cortical astrocytes. Glia 33:57–71.

Matthias K, Kirchhoff F, Seifert G, Hüttmann K, Matyash M, Kettenmann H, Steinhäuser C (2003) Segregated expression of AMPA-type glutamate receptors and glutamate transporters defines distinct astrocyte populations in the mouse hippocampus. J Neurosci 23:1750–1758.

Megias M, Emri Z, Freund TF, Gulyas AI (2001) Total number and distribution of inhibitory and excitatory synapses on hippocampal CA1 pyramidal cells. Neuroscience 102:527–540.

Millar JA, Barratt L, Southan AP, Page KM, Fyffe REW, Robertson B, Mathie A (2000) A functional role for the two-pore domain potassium channel TASK-1 in cerebellar granule neurons. Proc Natl Acad Sci U S A 97:3614–3618.

Mulligan SJ, MacVicar BA (2004) Calcium transients in astrocyte endfeet cause cerebrovascular constrictions. Nature 431:195–199.

Nagelhus EA, Mathiisen TM, Ottersen OP (2004) Aquaporin-4 in the central nervous system: cellular and subcellular distribution and coexpression with KIR4.1. Neuroscience 129:905–913.

Neusch C, Rozengurt N, Jacobs RE, Lester HA, Kofuji P (2001) Kir4.1 potassium channel subunit is crucial for oligodendrocyte development and *in vivo* myelination. J Neurosci 21:5429–5438.

Neusch C, Papadopoulos N, Müller M, Maletzki I, Winter SM, Hirrlinger J, Handschuh M, Bähr M, Richter DW, Kirchhoff F, Hülsmann S (2005) Lack of the Kir4.1 channel subunit abolishes K+ buffering properties of astrocytes in the ventral respiratory group: impact on extracellular K+ regulation. J Neurophysiol 95:1843–1852.

Newman E, Reichenbach A (1996) The Muller cell: a functional element of the retina. Trends Neurosci 19:307–312.

Nolte C, Matyash M, Pivneva T, Schipke CG, Ohlemeyer C, Hanisch UK, Kirchhoff F, Kettenmann H (2001) GFAP promoter-controlled EGFP-expressing transgenic mice: a tool to visualize astrocytes and astrogliosis in living brain tissue. Glia 33:72–86.

Olsen ML, Higashimori H, Campbell SL, Hablitz JJ, Sontheimer H (2006) Functional expression of Kir4.1 channels in spinal cord astrocytes. Glia 53:516–528.

Orkand RK (1986) Glial-interstitial fluid exchange. Ann N Y Acad Sci 481:269–272.

Päsler D, Gabriel S, Heinemann U (2007) Two-pore-domain potassium channels contribute to neuronal potassium release and glial potassium buffering in the rat hippocampus. Brain Res 1173:14–26.

Patel AJ, Honoré E, Maingret F, Lesage F, Fink M, Duprat F, Lazdunski M (1998) A mammalian two pore domain mechano-gated S-like K+ channel. EMBO J 17:4283–4290.

Pessia M, Tucker SJ, Lee K, Bond CT, Adelman JP (1996) Subunit positional effects revealed by novel heteromeric inwardly rectifying K+ channels. EMBO J 15:2980–2987.

Poopalasundaram S, Knott C, Shamotienko OG, Foran PG, Dolly JO, Ghiani CA, Gallo V, Wilkin GP (2000) Glial heterogeneity in expression of the inwardly rectifying K+ channel, Kir4.1, in adult rat CNS. Glia 30:362–372.

Rusznak Z, Pocsai K, Kovacs I, Por A, Pal B, Biro T, Szucs G (2004) Differential distribution of TASK-1, TASK-2 and TASK-3 immunoreactivities in the rat and human cerebellum. Cell Mol Life Sci 61:1532–1542.

Schröder W, Hager G, Kouprijanova E, Weber M, Schmitt AB, Seifert G, Steinhäuser C (1999) Lesion-induced changes of electrophysiological properties in astrocytes of the rat dentate gyrus. Glia 28:166–174.

Schröder W, Seifert G, Hüttmann K, Hinterkeuser S, Steinhäuser C (2002) AMPA receptor-mediated modulation of inward rectifier K(+) channels in astrocytes of mouse hippocampus. Mol Cell Neurosci 19:447–458.

Seifert G, Steinhäuser C (1995) Glial cells in the mouse hippocampus express AMPA receptors with an intermediate Ca^{2+} permeability. Eur J Neurosci 7:1872–1881.

Seifert G, Rehn L, Weber M, Steinhäuser C (1997) AMPA receptor subunits expressed by single astrocytes in the juvenile mouse hippocampus. Mol Brain Res 47:286–294.

Seifert G, Schilling K, Steinhauser C (2006) Astrocyte dysfunction in neurological disorders: a molecular perspective. Nat Rev Neurosci 7:194–206.

Shimada M, Akagi N, Goto H, Watanabe H, Nakanishi M, Hirose Y, Watanabe M (1992) Microvessel and astroglial cell densities in the mouse hippocampus. J Anat 180:89–95.

Skatchkov SN, Eaton MJ, Shuba YM, Kucheryavykh YV, Derst C, Veh RW, Wurm A, Iandiev I, Pannicke T, Bringmann A, Reichenbach A (2006) Tandem-pore domain potassium channels are functionally expressed in retinal (Muller) glial cells. Glia 53:266–276.

Steinhäuser C, Berger T, Frotscher M, Kettenmann H (1992) Heterogeneity in the membrane current pattern of identified glial cells in the hippocampal slice. Eur J Neurosci 4:472–484.

Steinhäuser C, Jabs R, Kettenmann H (1994) Properties of GABA and glutamate responses in identified glial cells of the mouse hippocampal slice. Hippocampus 4:19–36.

Takumi T, Ishii T, Hori Y, Morishige K-I, Takahashi N, Yamada M, Yamashita T, Kiyama H, Sohmiya K, Nakanishi S, Kurachi Y (1995) A novel ATP-dependent inward rectifier potassium channel expressed predominantly in glial cells. J Biol Chem 270:16339–16346.

Tanemoto M, Kittaka N, Inanobe A, Kurachi Y (2000) In vivo formation of a proton-sensitive K$^+$ channel by heteromeric subunit assembly of Kir5.1 with Kir4.1. J Physiol 525:587–592.

Volterra A, Meldolesi J (2005) Astrocytes, from brain glue to communication elements: the revolution continues. Nat Rev Neurosci 6:626–640.

Wallraff A, Odermatt B, Willecke K, Steinhäuser C (2004) Distinct types of astroglial cells in the hippocampus differ in gap junction coupling. Glia 48:36–43.

Wallraff A, Kohling R, Heinemann U, Theis M, Willecke K, Steinhäuser C (2006) The impact of astrocytic gap junctional coupling on potassium buffering in the hippocampus. J Neurosci 26:5438–5447.

Walz W (2000) Role of astrocytes in the clearance of excess extracellular potassium. Neurochem Int 36:291–300.

Wen H, Nagelhus EA, Amiry-Moghaddam M, Agre P, Ottersen OP, Nielsen S (1999) Ontogeny of water transport in rat brain: postnatal expression of the aquaporin-4 water channel. Eur J Neurosci 11:935–945.

Wigley R, Hamilton N, Nishiyama A, Kirchhoff F, Butt AM (2007) Morphological and physiological interactions of NG2-glia with astrocytes and neurons. J Anat 210:661–670.

Wurm A, Pannicke T, Iandiev I, Wiedemann P, Reichenbach A, Bringmann A (2006) The developmental expression of K+ channels in retinal glial cells is associated with a decrease of osmotic cell swelling. Glia 54:411–423.

Xu HX, Cui NR, Yang ZJ, Qu ZQ, Jiang C (2000) Modulation of Kir4.1 and Kir5.1 by hypercapnia and intracellular acidosis. J Physiol 524:725–735.

Zhou M, Kimelberg HK (2001) Freshly isolated hippocampal CA1 astrocytes comprise two populations differing in glutamate transporter and AMPA receptor expression. J Neurosci 21:7901–7908.

Zhou M, Schools GP, Kimelberg HK (2006) Development of GLAST(+) astrocytes and NG2(+) glia in rat hippocampus CA1: mature astrocytes are electrophysiologically passive. J Neurophysiol 95:134–143.